AD-A092 134 NAVAL POSTGRADUATE SCHOOL MONTEREY CA F/G 8/10
A STATISTICAL STUDY OF MONTHLY STORMINESS AND SEA SURFACE TEMPE--ETC(U
JUN 80 W H LITTLE

UNCLASSIFIED NL

1 OF 1
AD A092134

END
DATE FILMED
9-80
DTIC

(2)

# NAVAL POSTGRADUATE SCHOOL

## Monterey, California



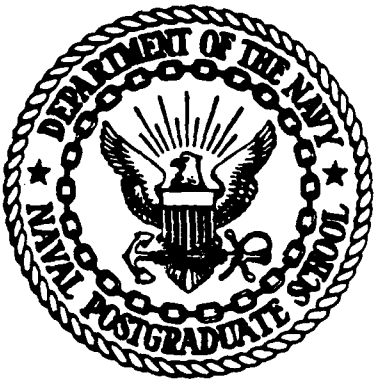




# THESIS

A STATISTICAL STUDY OF MONTHLY STORMINESS AND SEA SURFACE TEMPERATURE ANOMALIES OVER THE NORTH PACIFIC OCEAN

by

William H. Little

June 1980

Thesis Advisor: R. L. Haney

Approved for public release; distribution unlimited.

SECURITY CLASSIFICATION OF THIS PAGE (When Data Entered)

| REPORT DOCUMENTATION PAGE | READ INSTRUCTIONS BEFORE COMPLETING FORM |
|---|---|
| 1. REPORT NUMBER | 2. GOVT ACCESSION NO. AD-A092 134 / 3. RECIPIENT'S CATALOG NUMBER |
| 4. TITLE (and Subtitle) A Statistical Study of Monthly Storminess and Sea Surface Temperature Anomalies over the North Pacific Ocean | 5. TYPE OF REPORT & PERIOD COVERED Master's Thesis; June 1980 |
| | 6. PERFORMING ORG. REPORT NUMBER |
| 7. AUTHOR(s) William H. Little | 8. CONTRACT OR GRANT NUMBER(s) |
| 9. PERFORMING ORGANIZATION NAME AND ADDRESS Naval Postgraduate School Monterey, California 93940 | 10. PROGRAM ELEMENT, PROJECT, TASK AREA & WORK UNIT NUMBERS |
| 11. CONTROLLING OFFICE NAME AND ADDRESS Naval Postgraduate School Monterey, California 93940 | 12. REPORT DATE June 1980 |
| | 13. NUMBER OF PAGES 81 |
| 14. MONITORING AGENCY NAME & ADDRESS(if different from Controlling Office) Naval Postgraduate School Monterey, California 93940 | 15. SECURITY CLASS. (of this report) Unclassified |
| | 15a. DECLASSIFICATION/DOWNGRADING SCHEDULE |

16. DISTRIBUTION STATEMENT (of this Report)

Approved for public release; distribution unlimited.

17. DISTRIBUTION STATEMENT (of the abstract entered in Block 20, if different from Report)

18. SUPPLEMENTARY NOTES

19. KEY WORDS (Continue on reverse side if necessary and identify by block number)

Air-Sea Interaction
Empirical Orthogonal Functions (EOF)
Anomalous Storminess

20. ABSTRACT (Continue on reverse side if necessary and identify by block number)

Empirical Orthogonal Function (EOF) and cross-correlation analysis were used to examine the interrelationships between anomalous wind forcing and anomalous sea surface temperature (SST) over the North Pacific Ocean for the period January 1969 through December 1978. Wind forcing was represented by $u_*^3$, friction velocity cubed, and $\text{curl}_z \tau$, wind stress curl, as computed from: (a) high-pass filtered (periods less than

DD FORM 1 JAN 73 1473 EDITION OF 1 NOV 68 IS OBSOLETE
S/N 0102-014-6601



SECURITY CLASSIFICATION OF THIS PAGE (When Data Entered)

ten days) wind components only, (b) a combination of high- and low-pass (periods greater than ten days) filtered wind components, and (c) the unfiltered (total) wind components. EOF analysis was applied to the monthly anomalies to extract "signal" from "noise." Lag correlation analysis was used to investigate the relations between anomalous wind values and SST.

It was found that both $u_*^3$ and $\mathrm{curl}_z \tau$ correlation maps show significant increases in correlations at zero and plus-one-month lag. (Large areas of the North Pacific Ocean were correlated at the 32% significance level and several smaller areas at 10%.) These relationships were somewhat stronger for $u_*^3$ than for $\mathrm{curl}_z \tau$ and stronger for the storm-related (filtered) parameters.

Approved for public release; distribution unlimited.

# A Statistical Study of Monthly Storminess and Sea Surface Temperature Anomalies over the North Pacific Ocean

by

William H. Little
Lieutenant Commander, United States Navy
B.S., University of Washington, 1971

Submitted in partial fulfillment of the
requirements for the degree of

MASTER OF SCIENCE IN METEOROLOGY AND OCEANOGRAPHY

from the

NAVAL POSTGRADUATE SCHOOL
June 1980

Author William H. Little

Approved by: Robert J. Haney
Thesis Advisor

Second Reader

G. J. Haltiner
Chairman, Department of Meteorology

William M. Tolles
Dean of Science and Engineering

## ABSTRACT

Empirical Orthogonal Function (EOF) and cross-correlation analysis were used to examine the interrelationships between anomalous wind forcing and anomalous sea surface temperature (SST) over the North Pacific Ocean for the period January 1969 through December 1978. Wind forcing was represented by $u_*^3$, friction velocity cubed, and $\mathrm{curl}_z\tau$, wind stress curl, as computed from: (a) high-pass filtered (periods less than ten days) wind components only, (b) a combination of high- and low-pass (periods greater than ten days) filtered wind components, and (c) the unfiltered (total) wind components. EOF analysis was applied to the monthly anomalies to extract "signal" from "noise." Lag correlation analysis was used to investigate the relations between anomalous wind values and SST.

It was found that both $u_*^3$ and $\mathrm{curl}_z\tau$ correlation maps show significant increases in correlations at zero and plus-one-month lag. (Large areas of the North Pacific Ocean were correlated at the 32% significance level and several smaller areas at 10%.) These relationships were somewhat stronger for $u_*^3$ than for $\mathrm{curl}_z\tau$ and stronger for the storm-related (filtered) parameters.

TABLE OF CONTENTS

LIST OF FIGURES

LIST OF TABLES

ACKNOWLEDGEMENTS

I would like to express my deepest appreciation to Dr. Robert L. Haney for his guidance, assistance and constructive criticism throughout the course of this research.

My appreciation is also extended to Dr. Jerome Namias of the Scripps Institution of Oceanography Climate Research Group who graciously provided the sea surface temperature data used in this study. Additionally, the personal assistance and guidance provided by Dr. R. W. Preisendorfer and Dr. Tim Barnett was of great value in guiding me through the testing for significance of the empirical orthogonal functions computed in this study.

Finally I wish to express my deepest thanks to my wife, Sally, for her patience, understanding and help.

# I. INTRODUCTION

This study is a statistical investigation using Empirical Orthogonal Function (EOF) analysis and cross correlation analysis to examine the interrelationships between anomalous wind forcing and anomalous sea surface temperatures (SST) over the North Pacific Ocean from 20°N to 60°N and 110°W to 130°E for the period January 1969 through December 1978. Particular attention is given to investigating the effect of surface wind components having time scales of ten days or less. The primary hypothesis to be tested in this research is that the sea surface temperature responds to atmospheric wind forcing, as manifested in storms, and that the amount of the response is proportional to the amount of wind forcing. No other surface temperature changing processes are included in this work. The concept for examining storminess comes from the strong relationship that exists between synoptic storms and air-sea exchange [Simpson (1969), Fissel, Pond and Miyake (1977), Elsberry and Camp (1978)]. In addition, Davis (1976), who examined the statistical relationship between monthly sea-level pressure anomalies and SST anomalies, suggested that anomalous atmospheric storminess might have a strong correlation to anomalous SST.

The approach and expectations of this study were that: (1) EOF analysis would be used to extract the essential features from the complex space-time patterns of wind and SST data, i.e., it would extract the "signal" from "noise" in the data, (2) correlation analysis would be used to examine relationships between the variables once the noise was removed, and (3) anomalous storminess values, computed in the form of friction velocity cubed and wind stress curl, would be significantly correlated with anomalous SST cooling.

The atmospheric data for this study were a special series of six-hourly surface wind analyses prepared by Fleet Numerical Oceanographic Center (FNOC). Friction velocity cubed ($u_*^3$) and the vertical component of the curl of the wind stress ($curl_z\tau$) were calculated because of the established relationship between $u_*^3$ and the mechanical mixing of the sea by the overlying atmosphere and the well-established relationship between $curl_z\tau$ and Ekman convergence and divergence. Monthly mean anomalies of $u_*^3$ and $curl_z\tau$ were computed using: (a) high-pass filtered (periods less than ten days) wind components only, (b) a combination of high- and low-pass (periods greater than 10 days) filtered wind components, and (c) the unfiltered (total) wind components. The partitioning of wind parameters into these three parts was designed to identify the effect of storms, both in isolation and in the presence of the existing mean

(low-pass) flow. Thus, six fields were created to represent the anomalous wind influence upon the ocean surface. EOF analysis of all data fields, including the anomalous SST values, was employed to extract the significant and almost noise-free "geophysical patterns." The resulting anomalous wind parameters were then correlated with the anomalous SST data at the time lags of minus three through plus three months to investigate possible temporal relationships.

The first topic considered below is data set description and analysis. It is followed by a discussion of EOF analysis and an explanation of the truncation scheme used to reduce noise. Then some observations are given on the lagged correlations of $u_*^3$ and SST, and $\mathrm{curl}_z \tau$ and SST. The statistical significance of the correlations is carefully examined and interpretations are made in light of that significance. Finally, some conclusions are drawn about the results produced.

## II. DATA SET DESCRIPTION AND ANALYSIS

### A. ACQUISITION AND ANOMALY COMPUTATION

#### 1. Sea Surface Temperature

Monthly sea surface temperature (SST) data for the period January 1969 through December 1978 were obtained from the Scripps Institution of Oceanography Climate Research Group through the generosity of Jerome Namias and Robert Born. The geographical orientation of these data as delineated in Figure 1 was a nine by twenty-five array utilizing the 5° square grid used by Namias' group which extends from 20°N to 60°N and 110°W to 130°E. Due to missing data during the 120-month record at some of the 225 grid points, only 166 grid points were retained for analysis. The small squares and circles in Figure 1 show these 166 points. At these points, only 79 discrete values were missing out of the total 19,920 possible. These missing values were filled by temporally interpolating between the preceding and following monthly values. All SST values were converted from Fahrenheit to Centigrade and then processed to compute anomalies. The computation of monthly anomalies from all data sets in this study was accomplished by finding the difference between the observed monthly value and the 10-year average value found at the same grid point and month of year as the observation.

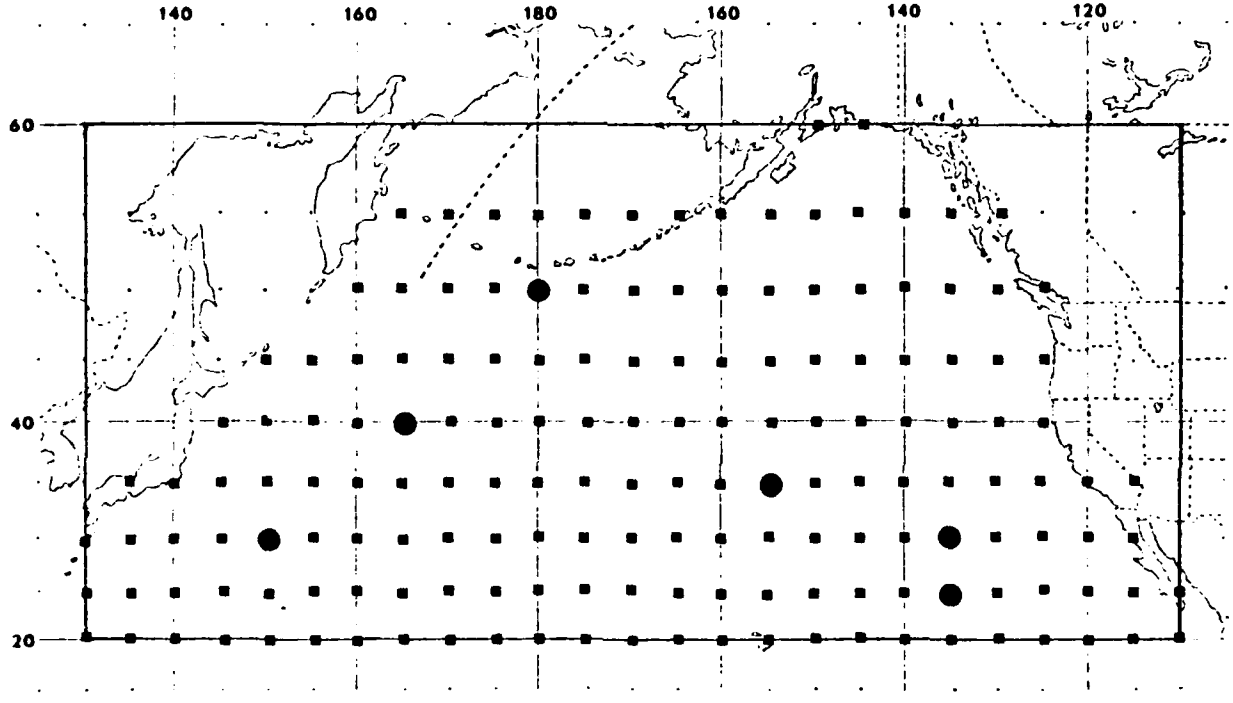


Figure 1. Data grid with 166 retained points delineated by squares and circles.

2. Friction Velocity and Surface Stress

In addition to SST, six anomalous surface wind parameters were investigated. Three involved $u_*^3$ where $u_*$ is the friction velocity and three involved $\text{curl}_z\tau$ where $\tau$ is the surface stress. These were obtained from Haney, Risch and Heise (1980), which in turn was based in part on the earlier thesis by Risch (1980). They used a special series of six-hourly surface wind analyses over the North Pacific Ocean prepared by Fleet Numerical Oceanographic Center (FNOC) covering the period January 1969 through December 1978 to analyze for synoptic storm activity. Temporal variance of the surface wind components at each grid point was "high-pass" filtered, thereby extracting all temporal variability having time scales less than ten days. The three $u_*^3$ and three $\text{curl}_z\tau$ data sets were then calculated using, respectively, (a) the total (unfiltered) wind components; (b) the high-pass wind components only; and (c) a combination of high- and low-pass wind components which represent the effects of storms (high-pass) in the presence of the existing mean (low-pass) field. See Haney, Risch and Heise (1980) for details. Having calculated the above wind parameters at every six-hourly observation over the entire 10-year period, monthly means, monthly climatologies over 10 years, and finally, monthly anomalies were constructed. The monthly anomalies, covering the same

10-year period as the SST anomalies, for the six wind-related data sets were then interpolated from the FNOC Northern Hemisphere Polar Stereographic grid to the same latitude-longitude grid points as the SST anomaly data.

B. DETRENDING AND STANDARDIZATION

The seven data sets representing monthly anomalies of $u_*^3 Fm$, $curl_z \tau Fm$ (both from total wind components), $u_*^3 F1$, $curl_z \tau F1$ (both from high-pass wind components only), $u_*^3 F2$, $curl_z \tau F2$ (both from high- and low-pass wind components) and SST were then detrended and standardized. The detrending equation was of the form

$$Y_m = y_m - (at_m + b)$$

where $Y_m$ is the detrended value at the $m^{th}$ time observation, $y_m$ is the original observation, a is the slope, b is the intercept and $t_m = (m - 1)\Delta t$, with $\Delta t$ = one month, being the time interval. This detrending was performed to remove all linear trends in the anomalies.

Standardization of the seven data sets was completed by using an equation of the form

$$X = \frac{x - \bar{x}}{s}$$

where X is the standardized value, x is the detrended value of the anomaly at a particular grid point, $\bar{x}$ is the time mean value of x, and s is the standard deviation of $x - \bar{x}$. The use of standardized variables assures that each variable at each grid point is of equal importance in determining the form of the field for comparison to other variable fields. Additionally, standardized anomaly fields of sea surface temperature and wind parameters correspond more closely to the climatological classifications of normal, above normal, much above normal, etc., than do the anomaly fields themselves [Kutzbach, 1967]. Standardization is required in order to utilize the EOF method of extracting "signal" from "noise," and it does not affect the subsequent correlation analysis.

The standard deviation maps of all seven data fields are included in Figures 2 through 4. Figure 2 shows that the centers of activity for the three $u_*^3$ data sets occurs eastward of Japan at about 45°N and 165°E. The largest changes of the curl fields in Figure 3 appear to be located about 50°N and 170°E. Finally, the standard deviation pattern of the SST data is indicated in Figure 4 with the most active area due east of Japan, 45°N and 150°E.

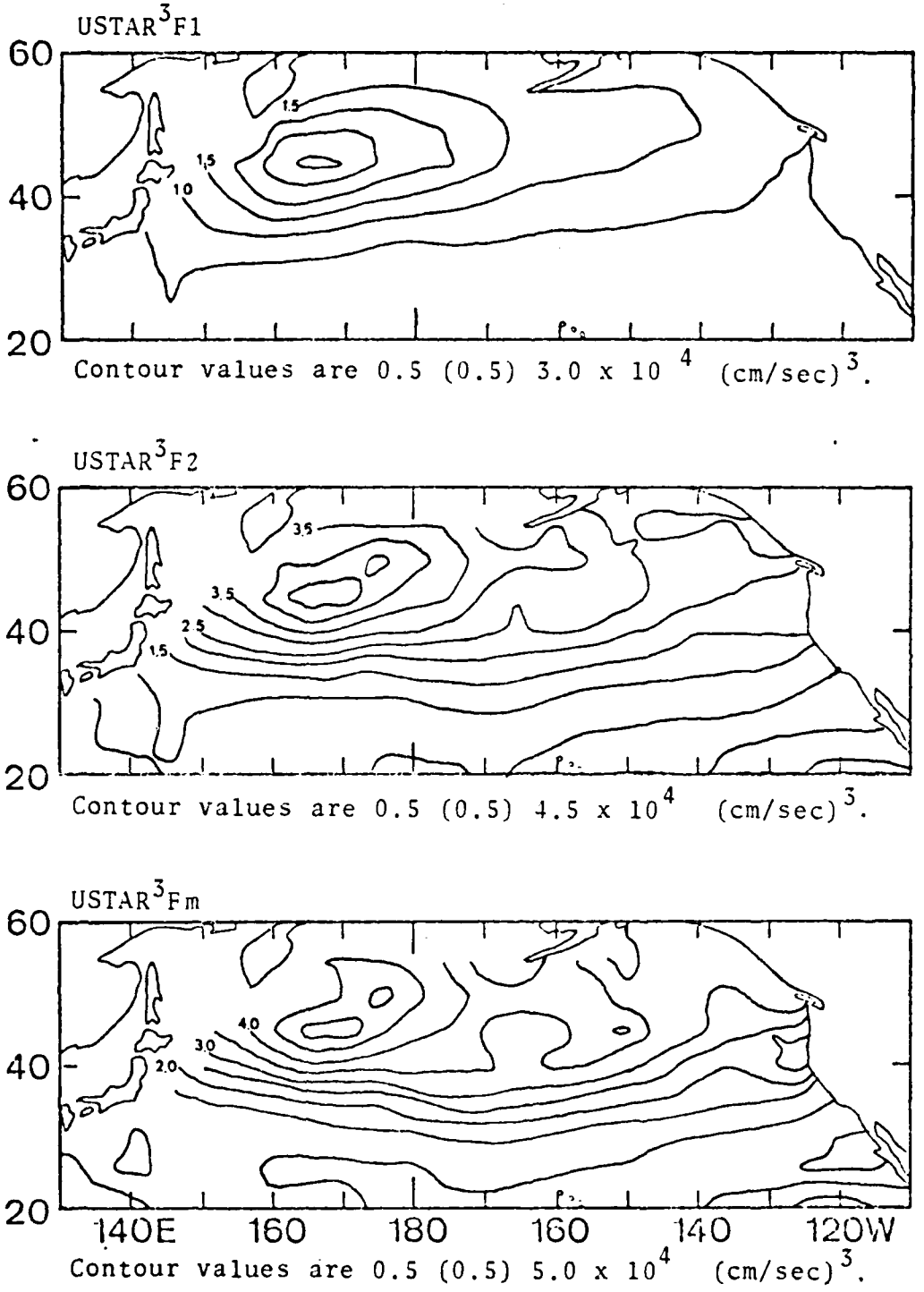


Figure 2. Contours of the standard deviation fields of the $u_*^3$ data.

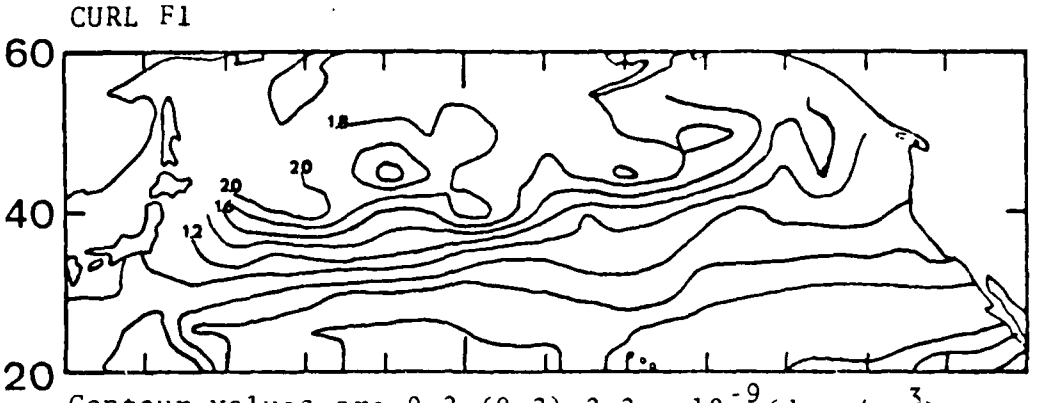


Contour values are 0.2 (0.2) 2.2 x $10^{-9}$ (dyne/$cm^3$).

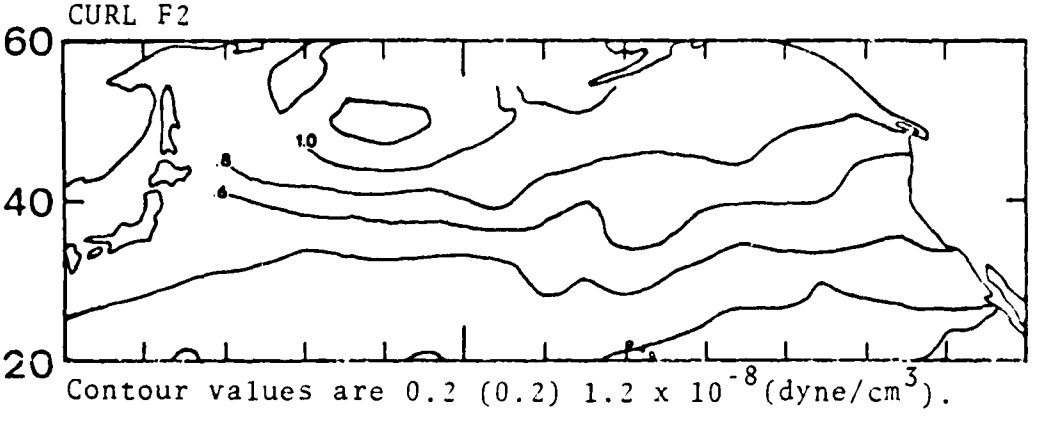


Contour values are 0.2 (0.2) 1.2 x $10^{-8}$ (dyne/$cm^3$).

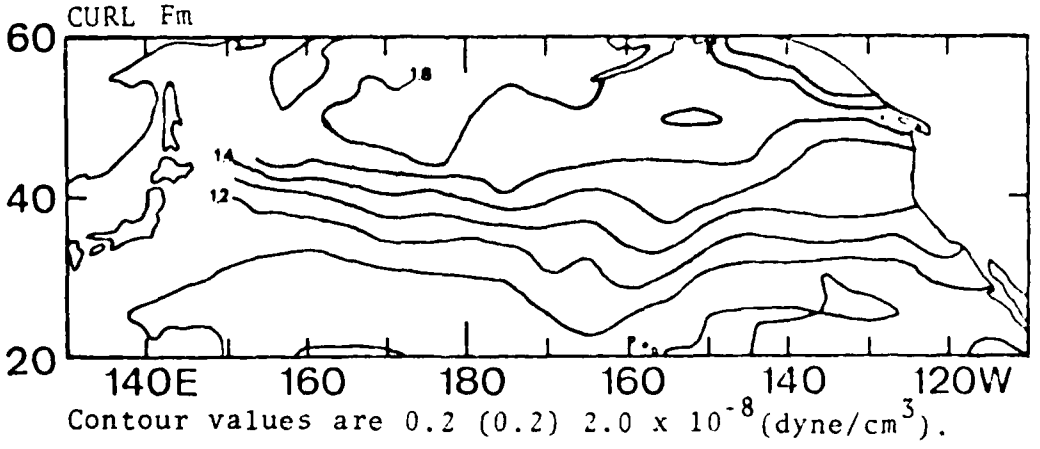


Contour values are 0.2 (0.2) 2.0 x $10^{-8}$ (dyne/$cm^3$).

Figure 3. Same as Fig. 2 except for curl data.

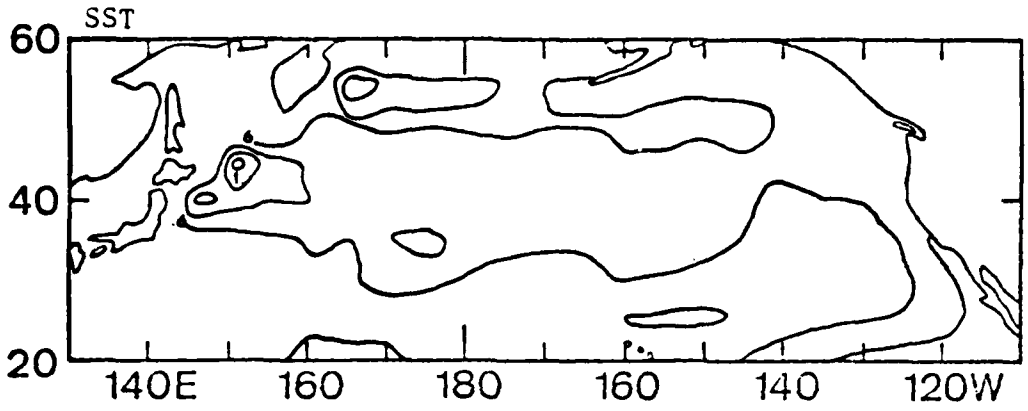


Contour values are .2, .4, .6, .8, 1.0, 1.2 (degrees C.).

Figure 4. Same as Fig. 2 except for SST data.

## III. CALCULATIONS PERFORMED

### A. EMPIRICAL ORTHOGONAL FUNCTION ANALYSIS

This research used empirical orthogonal function analysis to reduce a large number of highly correlated variables to a small number of independent variables. These are linear combinations of the original ones and contain a large percentage of the total variability. This technique has been used extensively in meteorology and oceanography [see, e.g., Kutzbach, 1967; Stidd, 1967; Davis, 1976; Weare, 1977; Harr, 1979] and, unlike most other orthogonal representations, this technique does not require a predetermined function, such as the Fourier components, sine and cosine, but depends upon the spatial and temporal interrelationships within the data being analyzed.

Kutzbach (1967) provides a lucid outline of the mathematical procedure necessary to define the orthogonal functions and their coefficients. A covariance (or correlation) matrix must be formed from the data set. To maximize the variance explained by the new functions, one must solve the system of linear equations associated with this covariance matrix for a set of eigenvalues. The eigenvalue represents the fraction of the total variance in the original data field explained by its corresponding eigenfunction. A function is found by substituting a given eigenvalue into

the system of equations and solving with the aid of an additional normalization condition. Just as the sines and cosines of Fourier analysis are space-orthogonal, the eigenfunctions produced by EOF analysis are also space-orthogonal. Associated with each function is a (time) coefficient which, when combined with the function and the result summed over all functions, provides an exact reproduction of the original field. That is,

$$X(x,t) = \sum_{m=1}^{120} A_m(t) EOF_m(x),$$

where $EOF_m$ is the eigenfunction, and $A_m$ is the time coefficient related to the $m^{th}$ eigenvalue. These coefficients, which are time-orthogonal [Kutzbach, 1967], are obtained from the functions and the original anomaly field. The specific formulations of the mathematics described here are detailed in the Appendix.

Figure 5 shows the cumulative percentage of variance explained versus eigenvalue mode number for the seven sets of data examined in this study. For all the seven data fields, the cumulative percent variance tends to increase logarithmically with the mode number. Mode number one is that spatial pattern which, in a least squares sense, explains the most variance possible (averaged over all grid points and time). That variance is between 9 and 19% of the

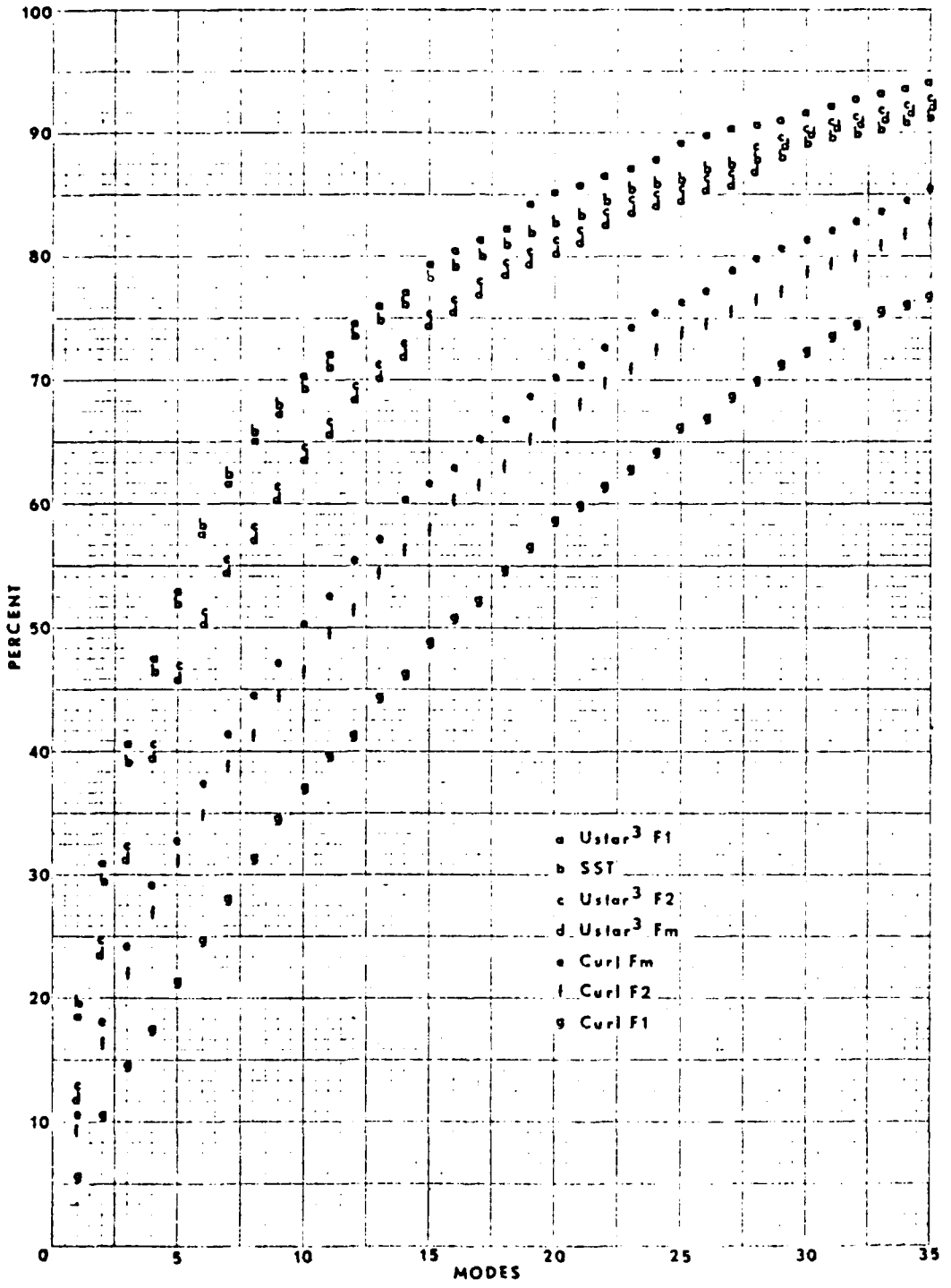


Figure 5. Cumulative percentage of total variance versus eigenvalue mode.

total variance depending on which of the seven fields is in question. It is significant that the cumulative variance explained by the SST and $u_*^3$ modes rises more rapidly than that of the curl$_z\tau$ modes. This means that the major part of the SST and $u_*^3$ fields can be explained by a few spatial modes while the curl variance is distributed more equally among a greater number of modes. The next section describes the method of determining, for each data variable, how many modes to retain for analysis.

## B. TRUNCATION METHOD AND SIGNIFICANCE LEVEL

Various investigators [Beale et al., 1967; Craddock and Flood, 1969; Farmer, 1971; Dyer, 1975; Rinne and Järvenoja, 1979] have suggested numerous methods for determining the point of truncation, i.e., finding the sufficient number of components of the series, given by the empirical orthogonal functions, to be retained for analysis. The choice of method depends largely on the purpose for which the empirical orthogonal function expansion is to be used. In this study, empirical orthogonal function analysis is used to reduce "noise." The term noise is defined here as that variability or randomness confined to small space scales, purely local effects, and observational errors. Recent numerical experiments by Preisendorfer and Barnett (1977) indicate that the classical asymptotic theory of random eigenvalues is inadequate to provide significance tests when the number P of

spatial data points is in the range of 10 to 100 (normally encountered in geophysical practice) and when the historical sample size N is in the similar range of 10 to 100. In the present study P = 166 and N = 120. Their experiments revealed that the asymptotic theory takes hold only for N on the order of 1000 or more for the above P values. After numerous experiments, Preisendorfer and Barnett have developed an empirical procedure for empirical orthogonal function truncation in the case of small sample sizes based on analysis of various arrays filled by Gaussian random variables of unit variance, zero mean. The procedure provides, for a given P and N, the significant confidence band for the randomly generated eigenvalues, thus providing the objective method of identifying the "noise" in a given data set. Tim Barnett generously computed and provided, for the specific N and P values in this study, the 5 and 95% confidence limits of eigenvalues for modes one to twenty-five. Figure 6 demonstrates the use of this truncation process for SST eigenvalues. The figure shows eigenvalues plotted against mode number on a semi-logarithmic grid. The first eigenvalue is always the largest, since the first EOF explains the most variance. The two solid curved lines labeled 95% and 5% represent the indicated range of the eigenvalues obtained by Barnett from one hundred repeated calculations using 166 by 120 arrays of random variables of unit variance. Thus,

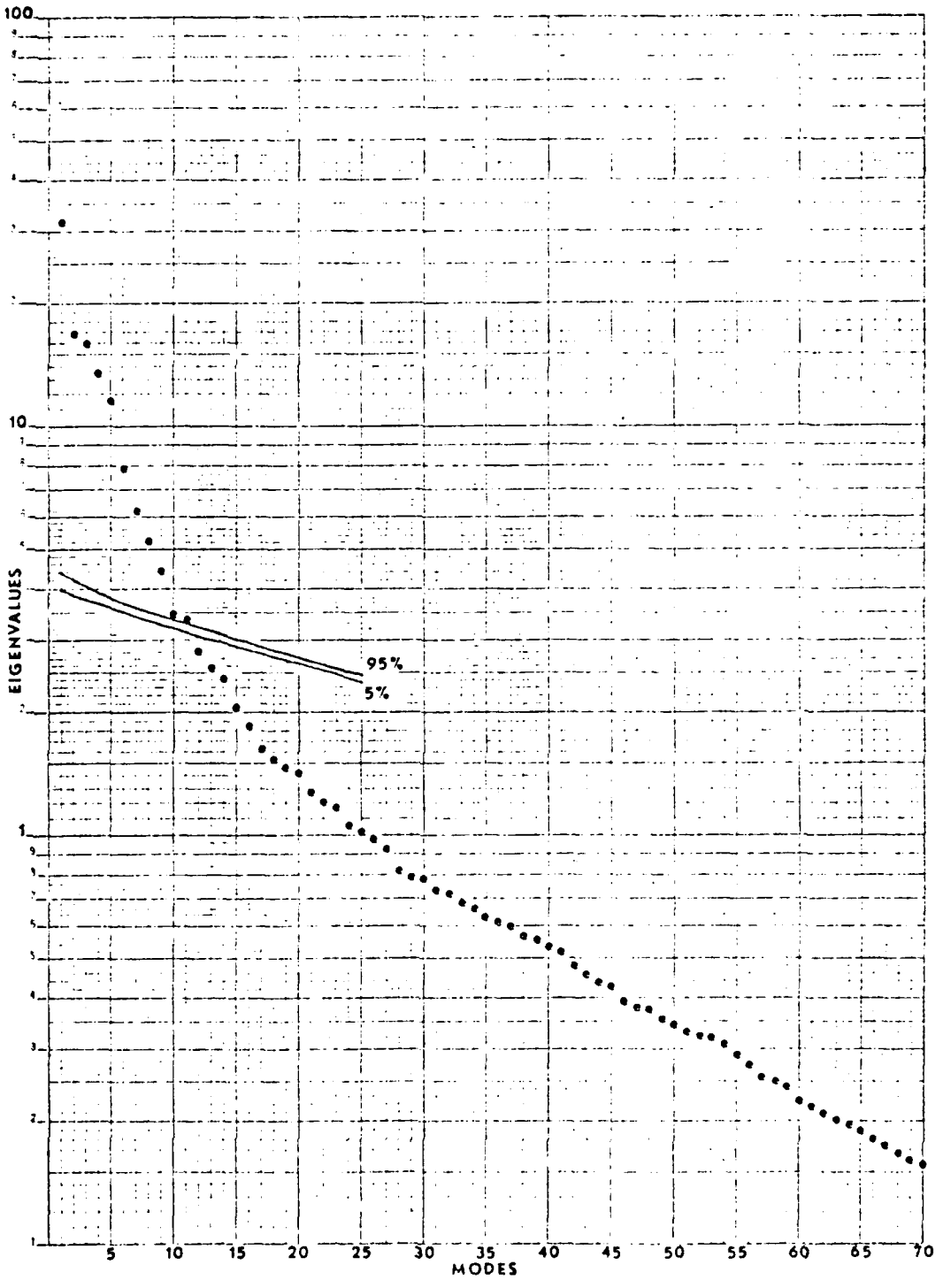


Figure 6. Eigenvalues of SST versus mode number. The 95% - 5% band indicates the truncation point (from Preisendorfer and Barnett).

TABLE 1

DATA FIELD RETAINED MODES AND CUMULATIVE PERCENTAGES

| Data Field | Number of Modes Retained | Percent Variance |
|---|---|---|
| SST | 11 | 72.29 |
| $Ustar^3 F1$ | 12 | 74.30 |
| $Ustar^3 F2$ | 15 | 75.30 |
| $Ustar^3 Fm$ | 15 | 75.82 |
| Curl F1 | 24 | 64.59 |
| Curl F2 | 18 | 63.70 |
| Curl Fm | 15 | 62.06 |

out of the 100 repeated experiments, 95% of the eigenvalues fell within the rather narrow band indicated by the two curves, with 5% above the top curve and 5% below the bottom curve. The e's represent the eigenvalues of the SST anomaly field, also standardized and, therefore, having unit variance. Notice that the arrays of random numbers have the variance spread rather evenly throughout the various modes while the SST field has much of its variance in the first ten or twenty out of the total of 120 modes. According to Preisendorfer and Barnett (1977), the method of extracting the "geophysical signal" from the SST data is to keep those empirical orthogonal function modes with eigenvalues lying above the 95% band created by the random data fields. In this case, only 5% of the retained field is likely to be attributable to random noise. In the case of the SST anomaly data, the first 11 modes were retained. This truncation procedure was applied to each data field with the results shown in Table I. Table I shows, for each data field, the number of empirical orthogonal function modes which were retained and the cumulative percent of the total variance which those modes explain.

Note that the data used in this study have a rather large amount of noise. The SST and $u_*^3$ anomaly fields are about 75% signal and 25% "noise," while the $\text{curl}_z \tau$ anomaly fields are only 62 to 65% "signal." There is more "noise" in the curl field because it is a spatial derivative of a quantity

(stress) which contains small-scale errors and large-scale geophysical variation.

Figure 7 is a comparison between the SST values at an individual grid point before and after EOF truncation. Curve (A) represents the detrended and standardized SST values from grid point number 84, located one-third of the way between Hawaii and the Aleutian Islands. Curve (B) represents the resultant values derived from the truncated EOF series for the same grid point. It should be noted that noise is reflected in (A) by the curve's rapid small-scale fluctuations. It is readily apparent that curve (B) is a damped form of curve (A). A considerable amount of the small-scale fluctuations have been eliminated with curve (B) still retaining the large-scale trends of curve (A).

In addition to the method described above, various other ways have been suggested for determining the point of truncation of the series given in EOFs. Rinne and Järvenoja (1979) have offered some of their own methods and summarized many others. These methods included: retaining eigenvalues which explain more than one percent of the total variance, retaining eigenvalues that are much larger than others, applying a statistical criterion based on a Bartlett's test to determine the values to be saved, and, finally, keeping all the largest eigenvalues which together account for 99% of the total variance. Another truncation test mentioned in this

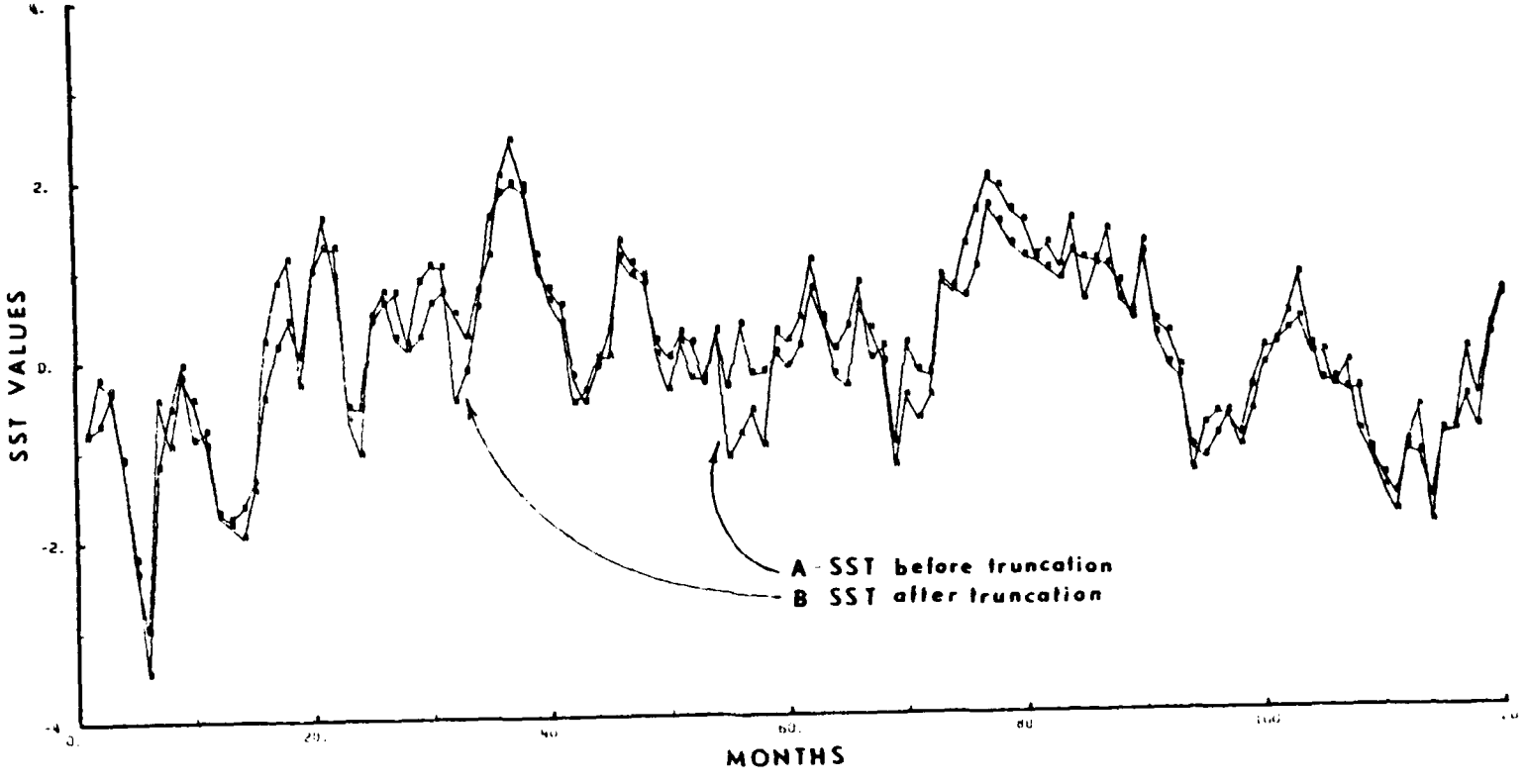


Figure 7. SST anomaly values at grid point 84 before and after truncation.

summarization is one which uses a diagram drafted similar to Figure 6 in this paper. The procedure truncates the EOF series at the largest eigenvalue at which the eigenvalue (versus mode number) curve can be approximated with a straight line. In Figure 6 the straight line approximation would start best at mode number twenty-four and thus, according to this method, the largest twenty-three eigenvalues would be retained.

All of the above methods would have retained more modes than the Preisendorfer and Barnett scheme which was used in this study. The choice of this scheme can best be explained by using a schematic of Rinne and Järvenoja (1979) shown in Figure 8.

The whole box represents the total variance and this consists of real environmental information (areas 1 and 2) and noise (areas 3 and 4), separated by the interior vertical line. EOF series truncation controls the placement of the sloping broken line which divides the box into an explained (areas 1 and 3) and unexplained (areas 2 and 4) portion The numbered areas are now identifiable as: (1) real information explained by EOFs, (2) real information EOFs fail to explain, (3) noise explained by EOFs, and (4) noise that EOFs fail to explain. (A) represents the situation when a relatively small number of EOFs are retained while (B) occurs when a relatively large number is saved. The Preisendorfer and

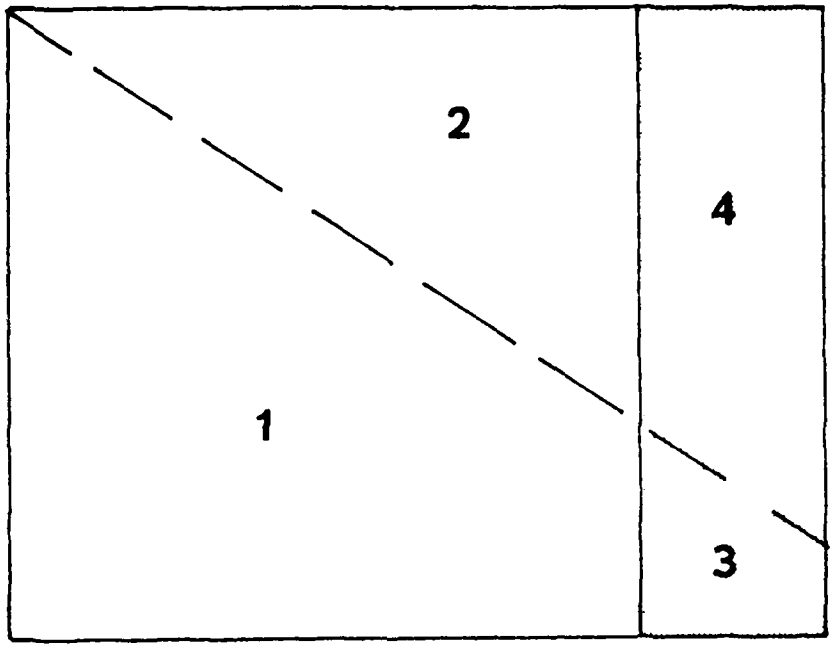


A

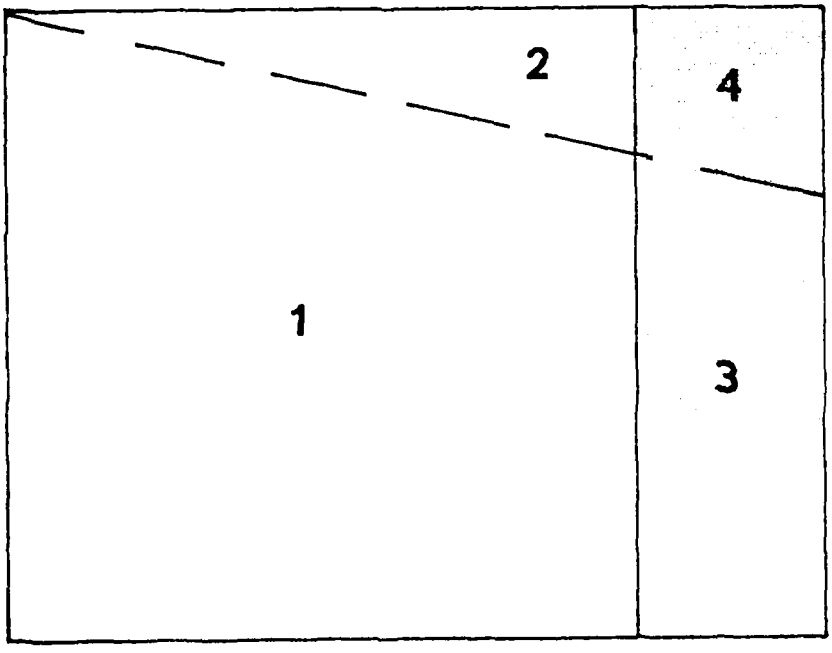


B

Figure 8. Box interpretation of the total variance where A is the case of saving a small number of terms and B is the case of retaining a large number of terms in the EOF series expansion.

Barnett (1977) method used in this study is closely represented by (A). Very little noise is retained at the "expense" of explaining a somewhat reduced amount of total variance. In the following section, possible relationships between the seven truncated anomaly data sets are examined.

# IV. RESULTS

## A. LAG CORRELATIONS BETWEEN $u_*^3$ AND SST

Figures 9 to 15 are maps of lagged correlations between $u_*^3$ and SST anomalies (detrended, standardized, and truncated) over the North Pacific Ocean. The map series steps through lags of minus three to plus three months, in one-month increments, with Figure 9 showing the minus-three-month case and Figure 15 ending the series with a plus-three-month lag between $u_*^3$ and SST. In the map series, SST is lagged relative to $u_*^3$. Thus, the map with a lag of minus three months shows the correlation between the $u_*^3$ field and the SST field that occurred three months before the $u_*^3$. In the opposite situation, the map lagged plus three months shows the correlation between the $u_*^3$ field and the SST field that occurred three months later. Each figure contains three maps, which are, from top to bottom, correlations between SST and (1) $u_*^3$F1 computed from high-pass wind components only, (2) $u_*^3$F2 computed from a combination of high- and low-pass wind components, and (3) $u_*^3$Fm computed from unfiltered (total) wind components, respectively. Finally, each map is shaded gray in areas of negative correlation values.

In anticipation that anomalous storminess values are related to anomalous surface cooling, it was expected that,

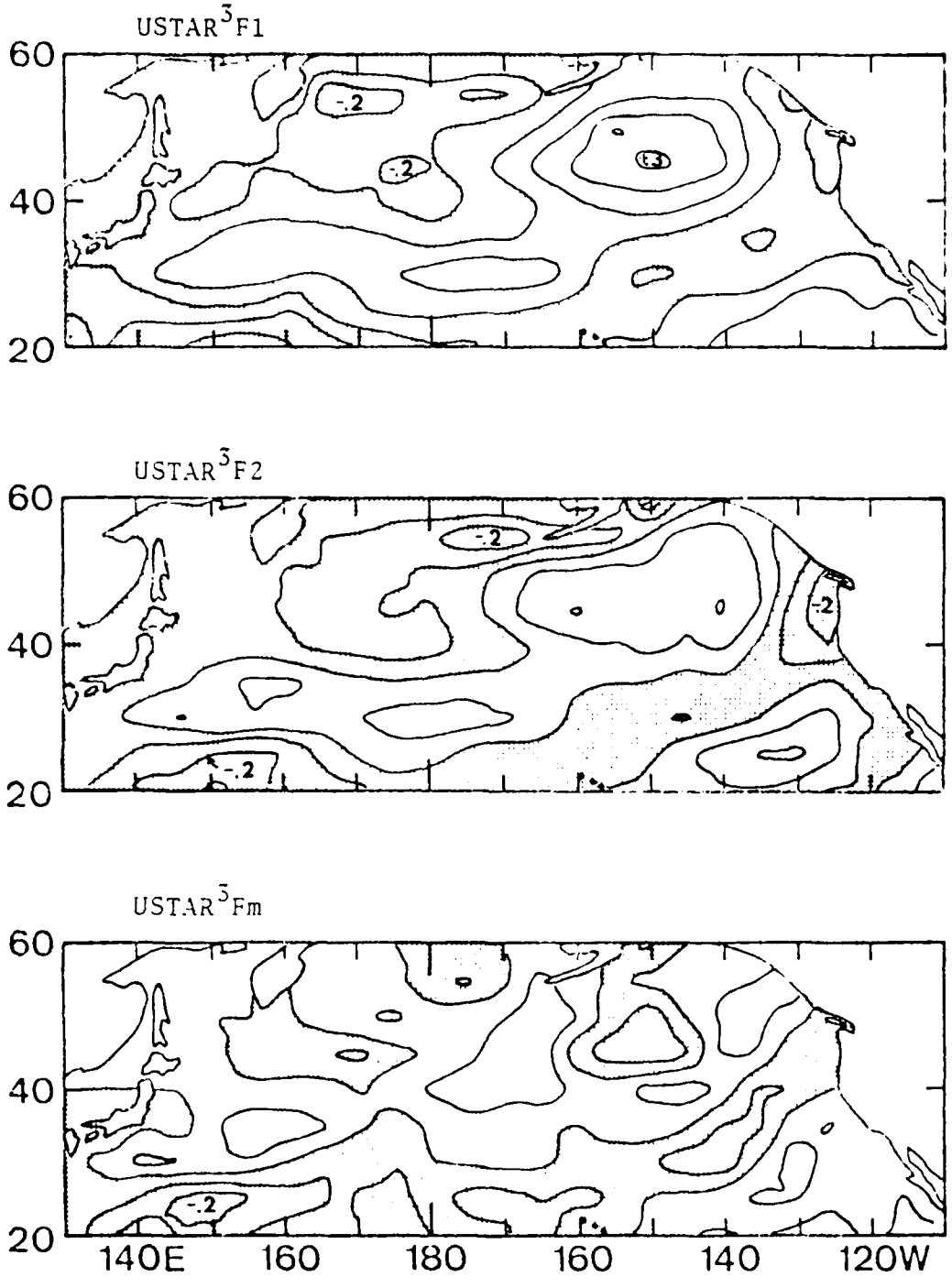


Figure 9. Correlation maps of the $u_*^3$ anomaly data fields with SST at a lag of minus three months. The last closed isoline is labeled in some regions having the largest correlations.

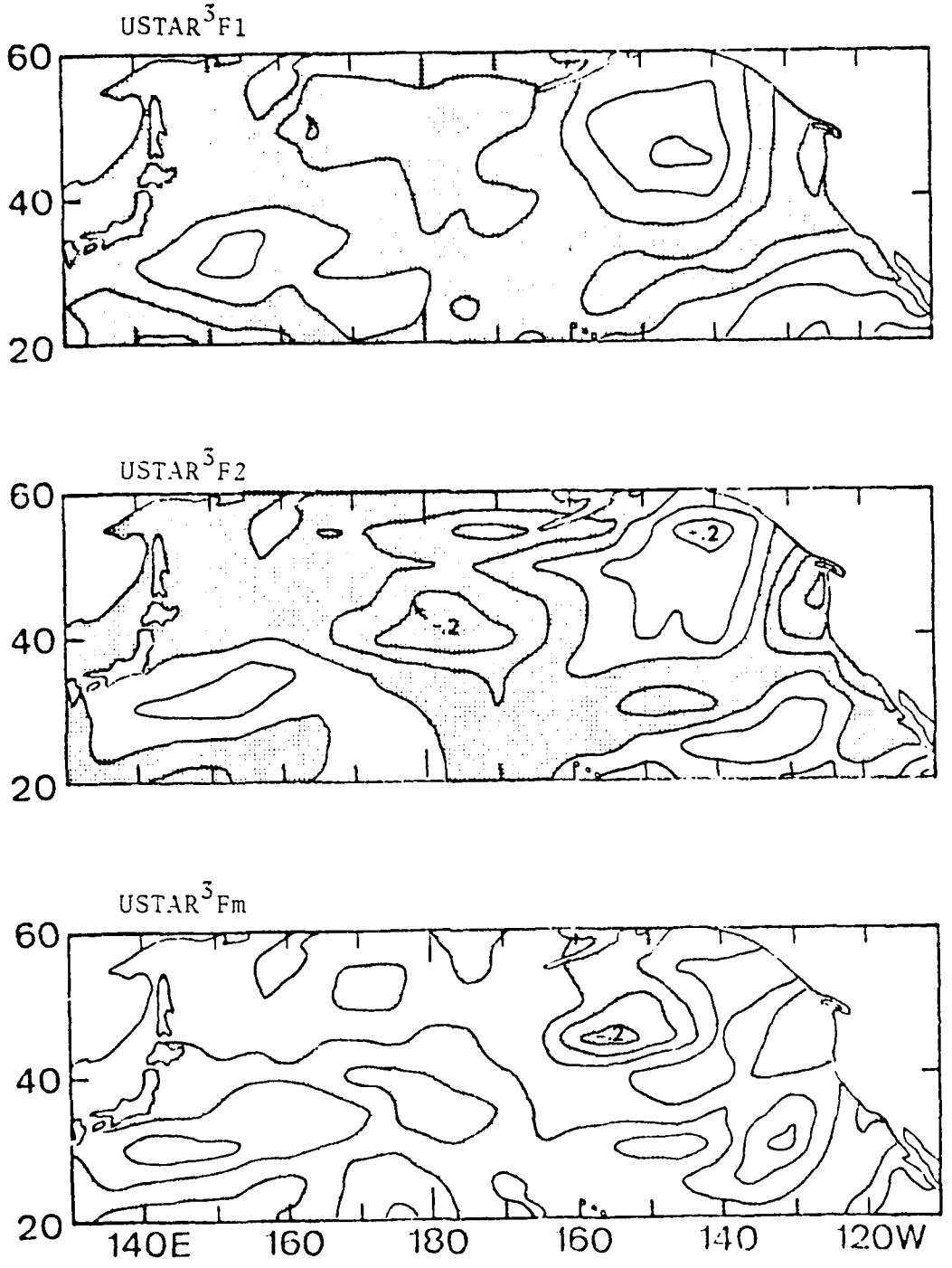


Figure 10. Same as Fig. 9 except lagged minus two months.

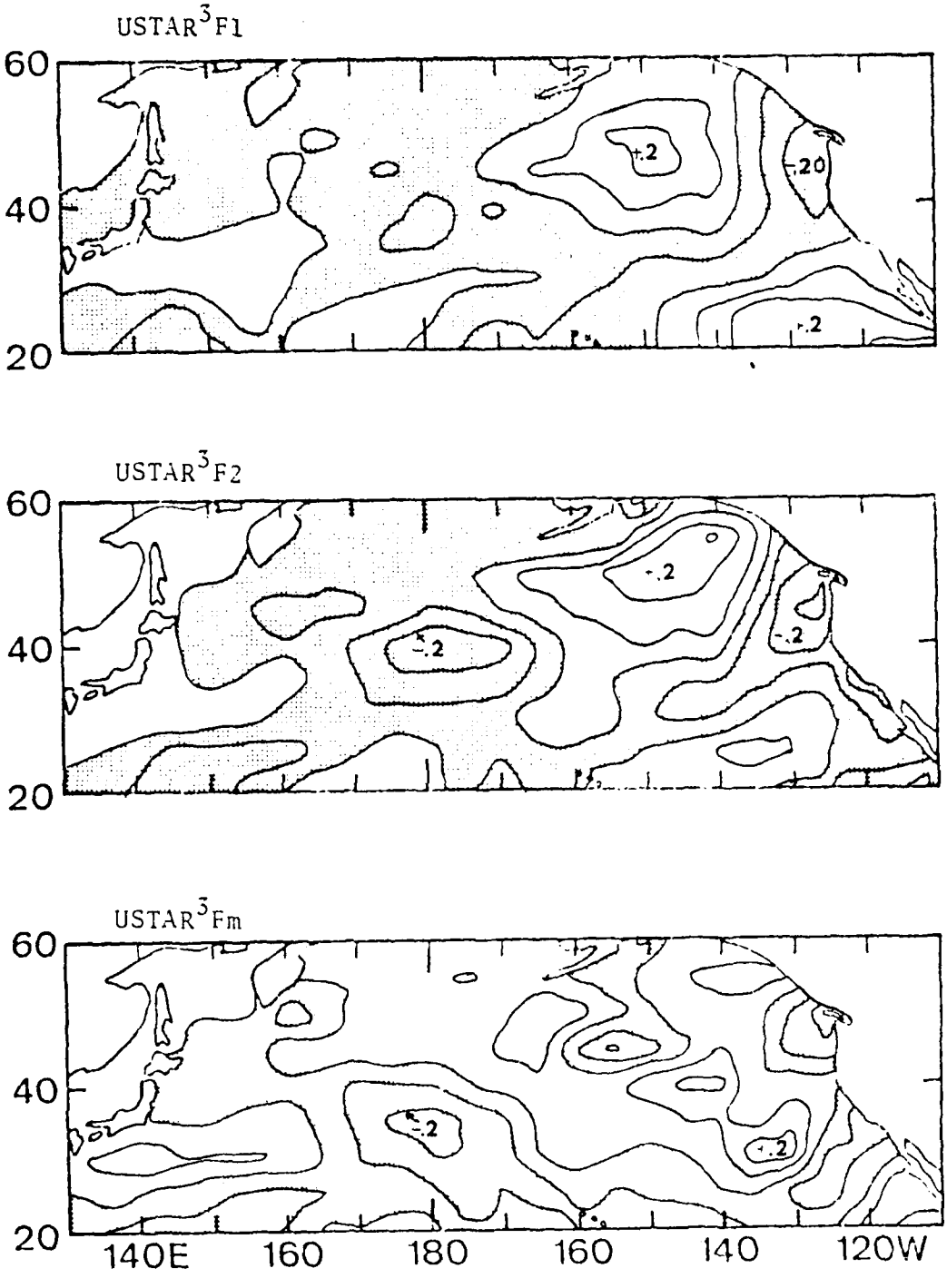


Figure 11. Same as Fig. 9 except lagged minus one month.

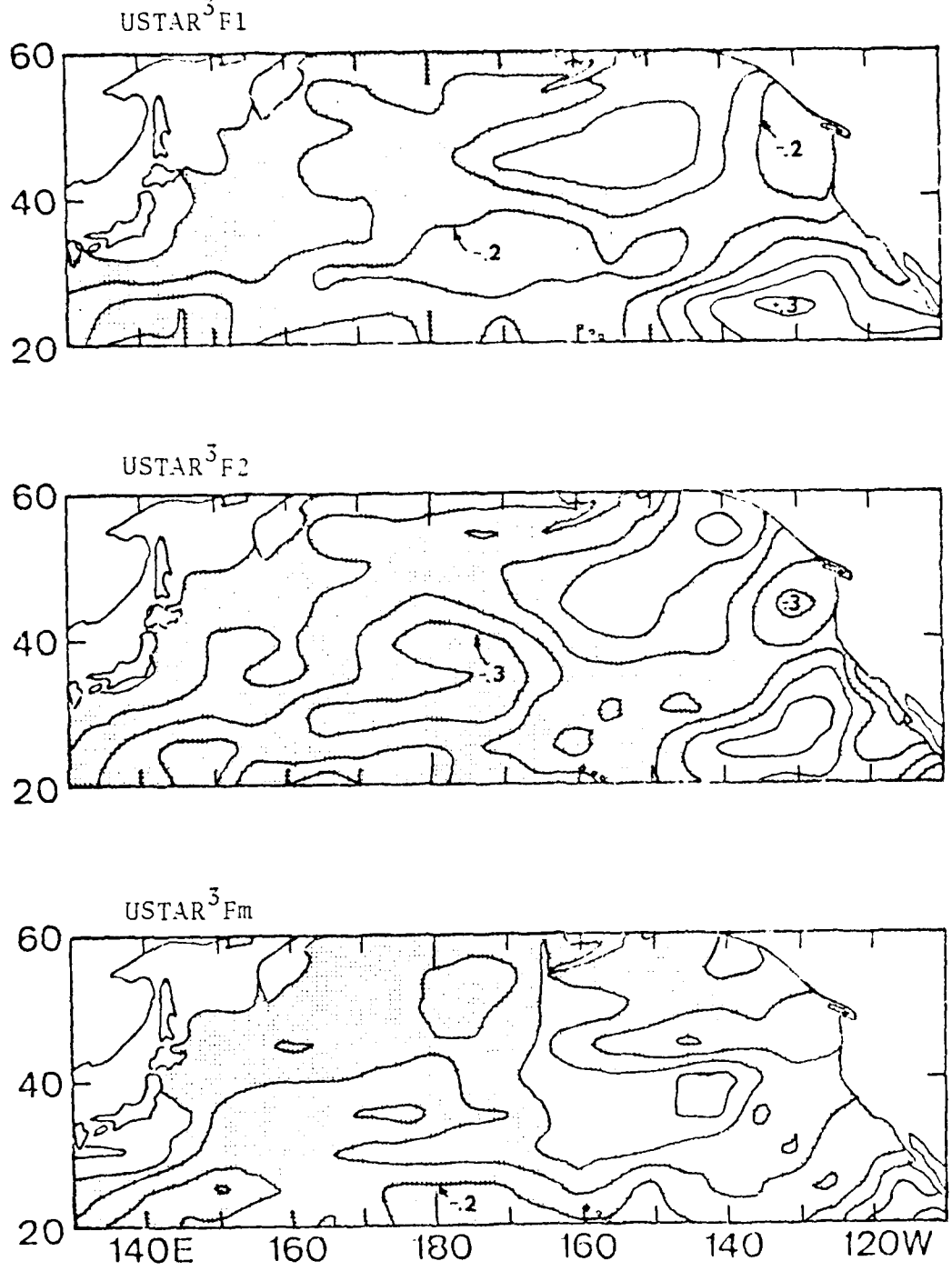


Figure 12. Same as Fig. 9 except no lag between data sets.

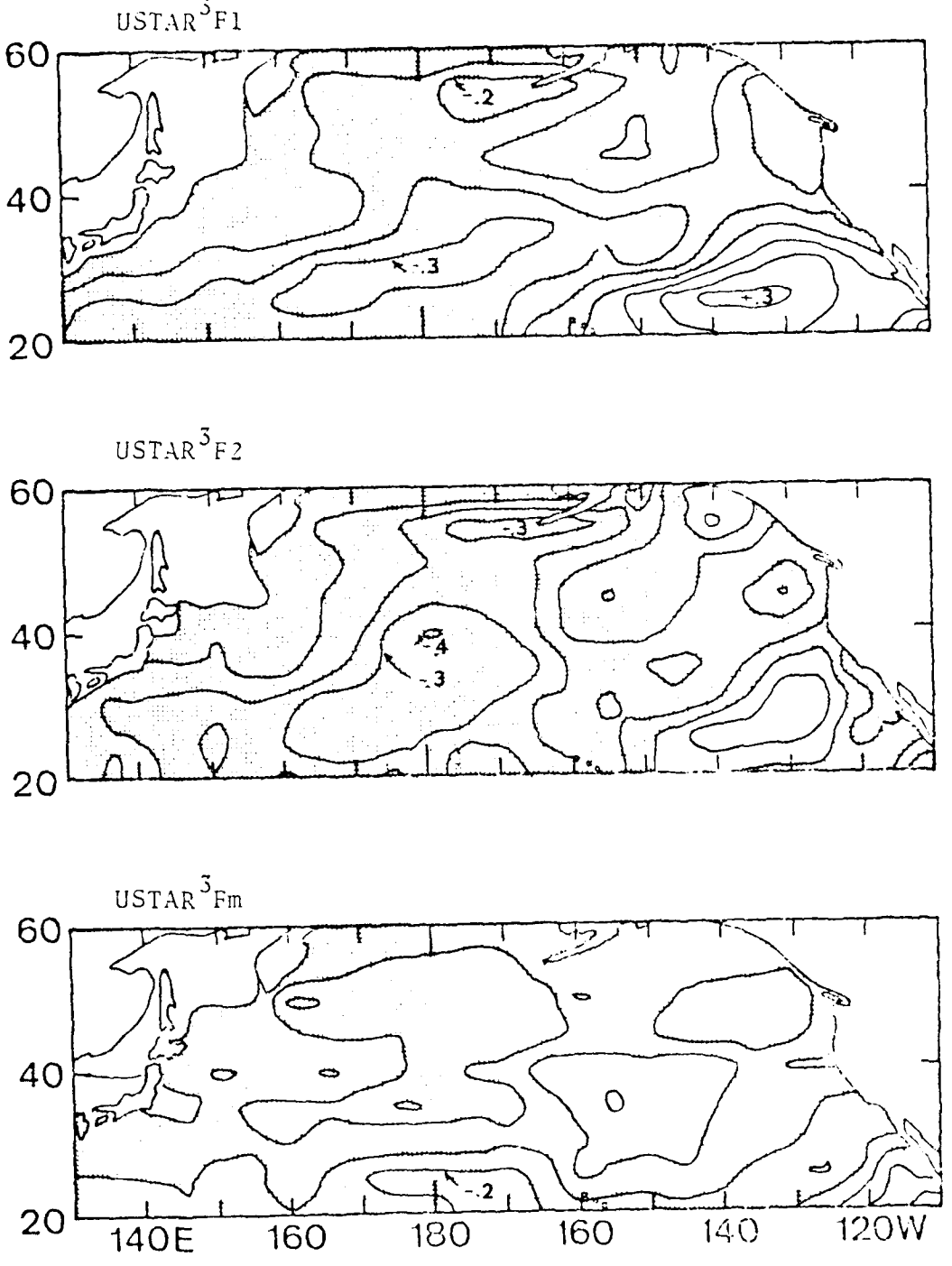


Figure 13. Same as Fig. 9 except lagged plus one month.

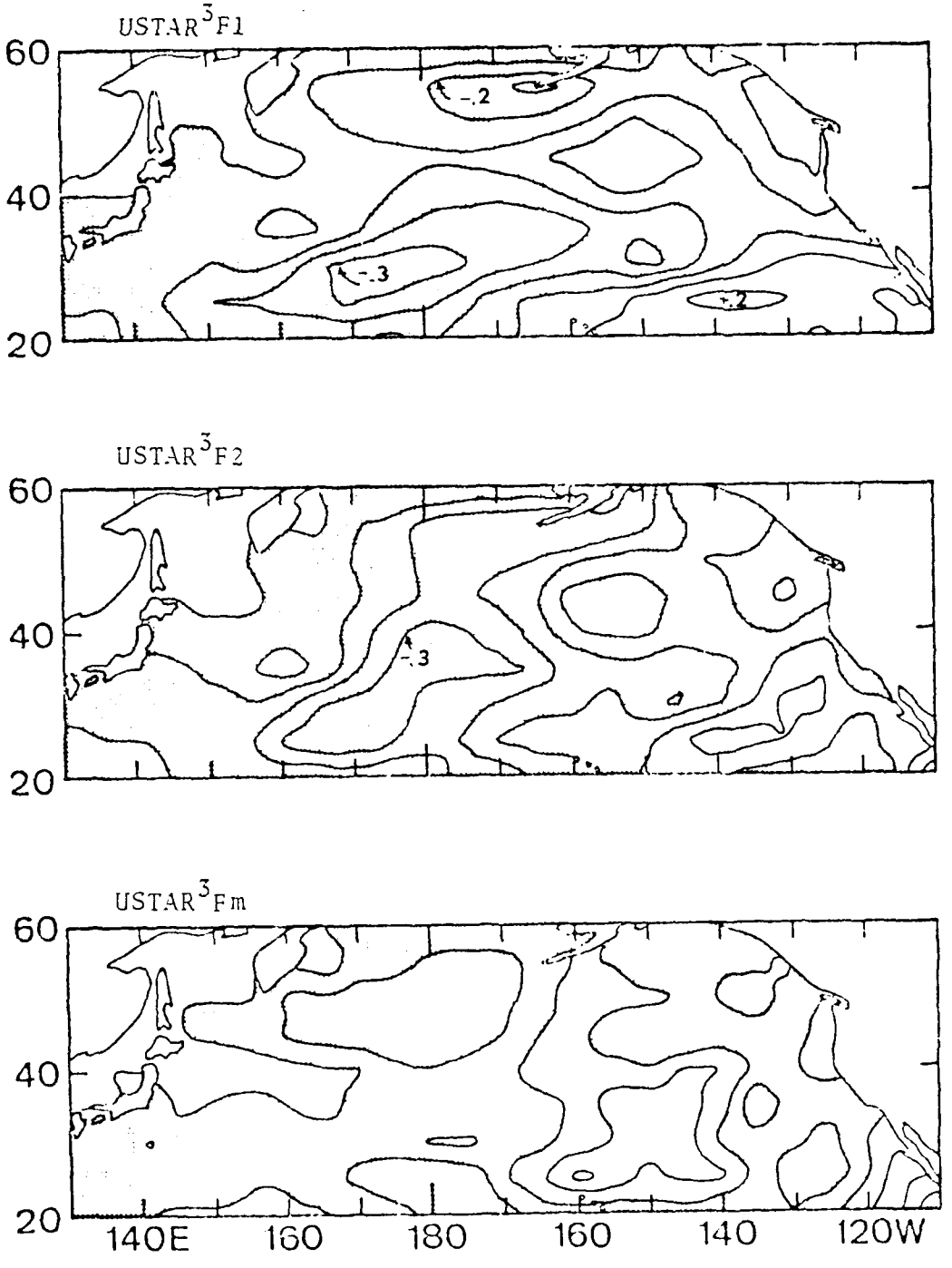


Figure 14. Same as Fig. 9 except lagged plus two months.

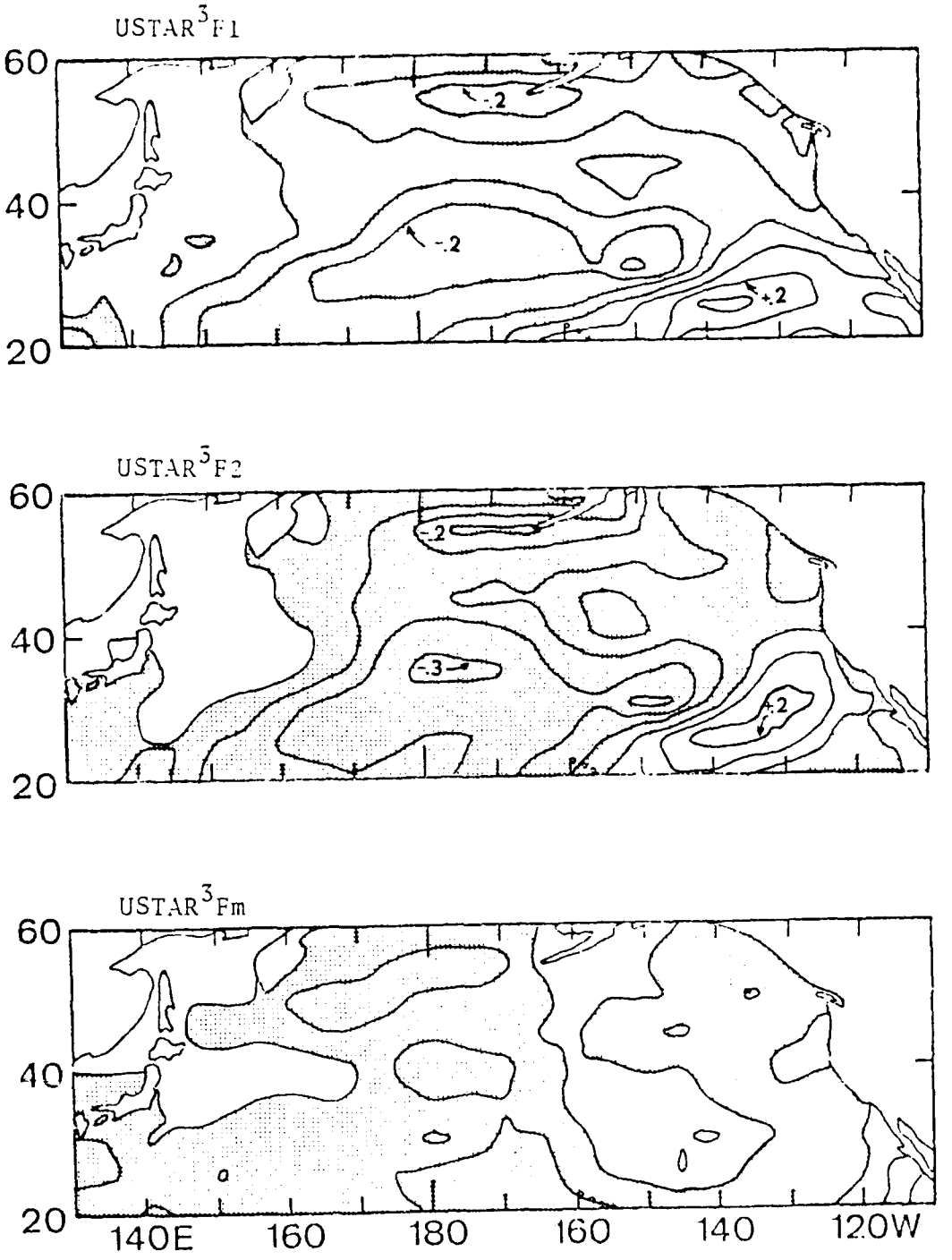


Figure 15. Same as Fig. 9 except lagged plus three months.

for lags greater than or equal to zero, maps would be mostly covered by negative correlation values. Examination of this $u_*^3$ series of maps reveals that a significant change occurs in the zero and plus-one-month lag maps. There is a visible increase in the gray shading, i.e., negative correlations, at these lags. Table II delineates some map parameters that can be used to quantify this increase in the negative correlation area when SST lags $u_*^3$. Almost without fail there are significant changes in going from the minus-one-month lag to the plus one. For instance, the sum of the negative correlations (RNEG) for $u_*^3$F2 goes from -10.81 at minus-one-month lag to -30.19 at plus-one-month lag. The number of grid points with negative correlations (NNEG) jumps from 99 at minus one to 143 at zero and then up to 147 at plus-one-month lag for $u_*^3$F2. The significance of this jump can be appreciated by considering a random correlation situation. In such a case, 83 grid points would be expected to have positive correlations and 83 would be expected to have negative correlations, with a standard deviation of 6.5 grid points. This is strictly true only if the grid points are independent of each other. This means that 68% of the time the number of negative points would lie between 76.5 and 89.5 and 95% of the time the number of negative points would lie between 70

TABLE II

CORRELATION MAP STATISTICS FOR ANOMALOUS $u_*^3$ LAGGED WITH ANOMALOUS SST

| | | LAG (MONTHS) | | | | | | |
|---|---|---|---|---|---|---|---|---|
| | | -3 | -2 | -1 | 0 | +1 | +2 | +3 |
| RNEG | $u_*^3$F1 | -11.53 | -10.68 | -9.00 | -20.42 | -24.96 | -18.30 | -15.48 |
| | $u_*^3$F2 | -10.59 | -9.87 | -10.81 | -26.34 | -30.19 | -22.15 | -19.20 |
| | $u_*^3$Fm | -7.46 | -7.66 | -10.35 | -18.24 | -16.53 | -9.34 | -9.11 |
| NNEG | $u_*^3$F1 | 97 | 109 | 98 | 133 | 131 | 127 | 115 |
| | $u_*^3$F2 | 94 | 101 | 99 | 143 | 147 | 140 | 129 |
| | $u_*^3$Fm | 76 | 87 | 86 | 131 | 139 | 110 | 120 |
| RPOS | $u_*^3$F1 | 7.74 | 5.35 | 5.98 | 5.16 | 5.92 | 5.04 | 6.53 |
| | $u_*^3$F2 | 7.20 | 6.15 | 5.85 | 1.88 | 1.86 | 1.97 | 3.63 |
| | $u_*^3$Fm | 6.81 | 6.58 | 6.55 | 2.66 | 1.89 | 4.48 | 2.74 |
| RSUM | $u_*^3$F1 | -3.79 | -5.32 | -3.02 | -15.27 | -19.05 | -13.26 | -8.94 |
| | $u_*^3$F2 | -3.39 | -3.72 | -4.97 | -24.46 | -28.33 | -20.18 | -15.57 |
| | $u_*^3$Fm | -.65 | -1.08 | -3.80 | -15.58 | -14.64 | -4.86 | -6.37 |

RNEG - Sum of Negative Correlations
NNEG - Number of Grid Points with a Negative Correlation
RPOS - Sum of Positive Correlations
RSUM - Arithmetic Sum of All Correlations

and 96. Thus, the increase of negative grid points from 99 to 147 is of notable significance.

Before continuing beyond this point, the issue of significance must be examined further. An issue of significance was raised and resolved earlier in this study when considering where to truncate the EOF series to ensure maximum signal and minimum noise. Thus, the correlations presented above are those associated with the geophysical fluctuations in SST and $u_*^3$ (i.e., the "signal") and are not attributable to error "noise." The paragraph preceding this one noted the significance of the changes that occurred in the correlation between negative and positive lags and provided mathematical evidence for this significance. The final significance to be examined is related to the existence of artificial correlation due to the interplay between the length of record examined and the dominant time scales of variation of the processes being studied.

As a first approximation to the magnitude of this possible artificial correlation, six grid points were chosen (circles in Fig. 1) and their temporal history of SST, computed after EOF truncation, was examined for repetitive events. (See Figures 16 through 21.) SST data were chosen to estimate the magnitude of the possible spurious correlations because it has relatively longer time scales of variability compared to the atmospheric fields. Table III shows

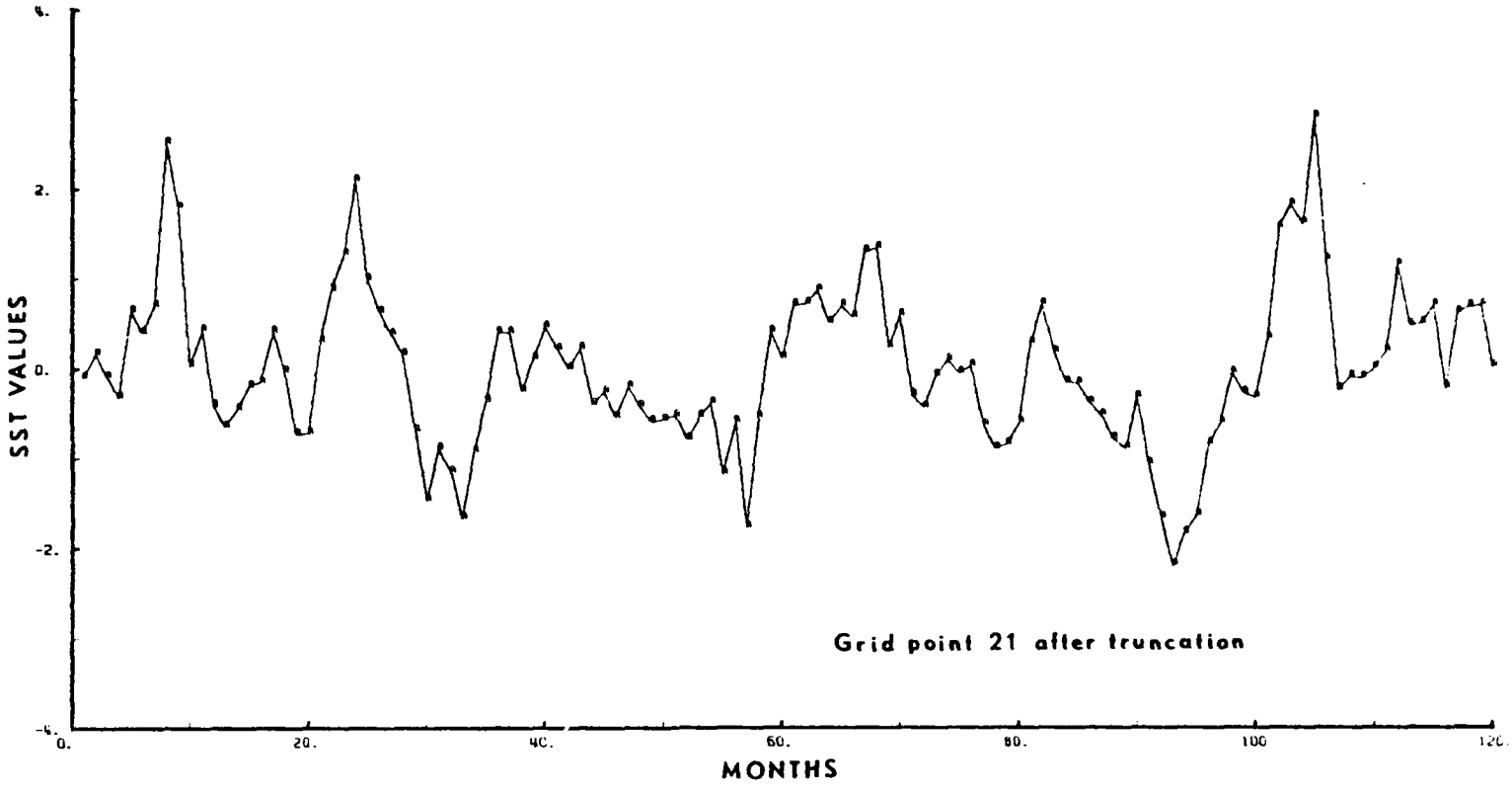


Figure 16. SST anomaly history at grid point 21 used for computation of artificial correlation.

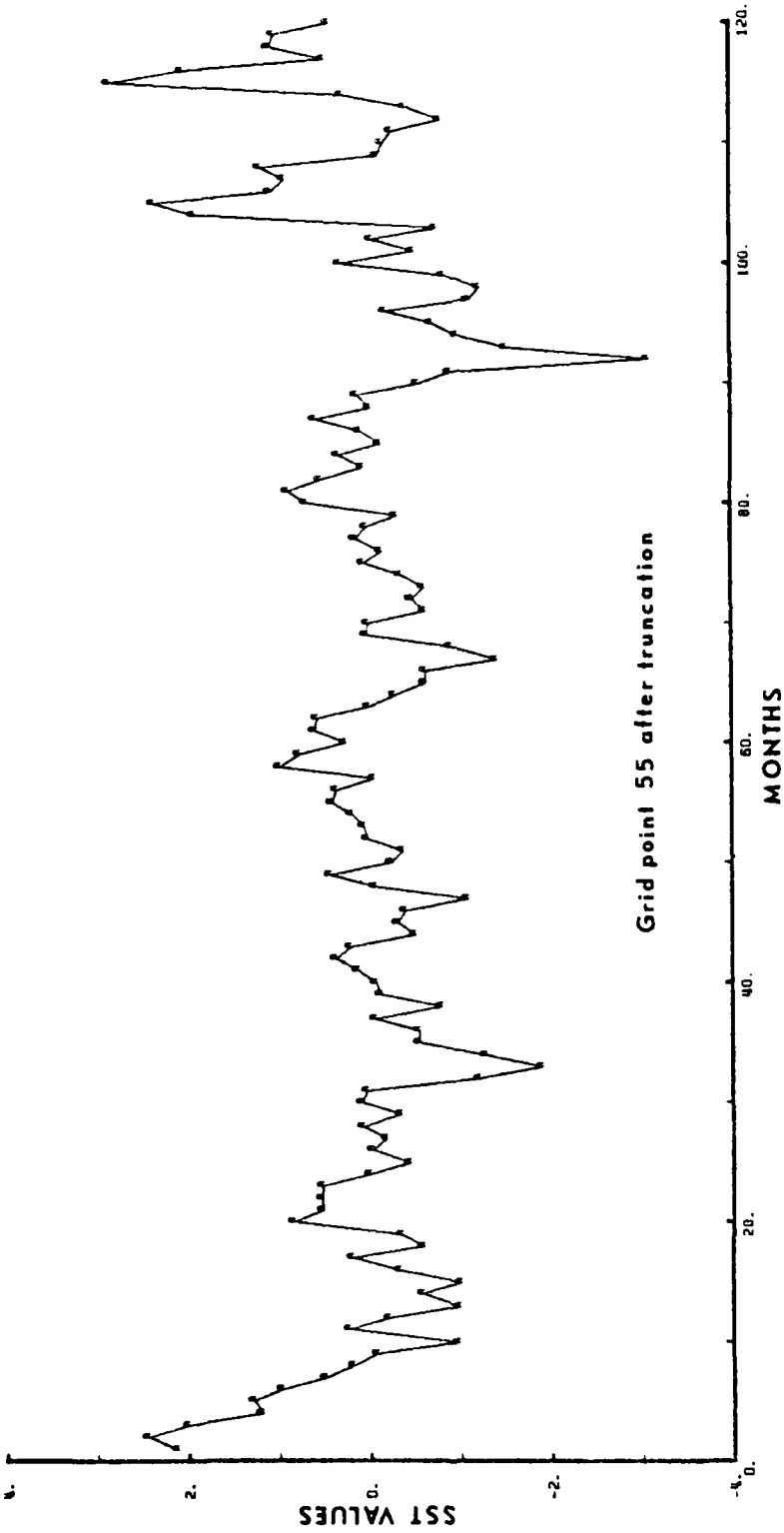


Figure 17. Same as Fig. 16 except for grid point 55.

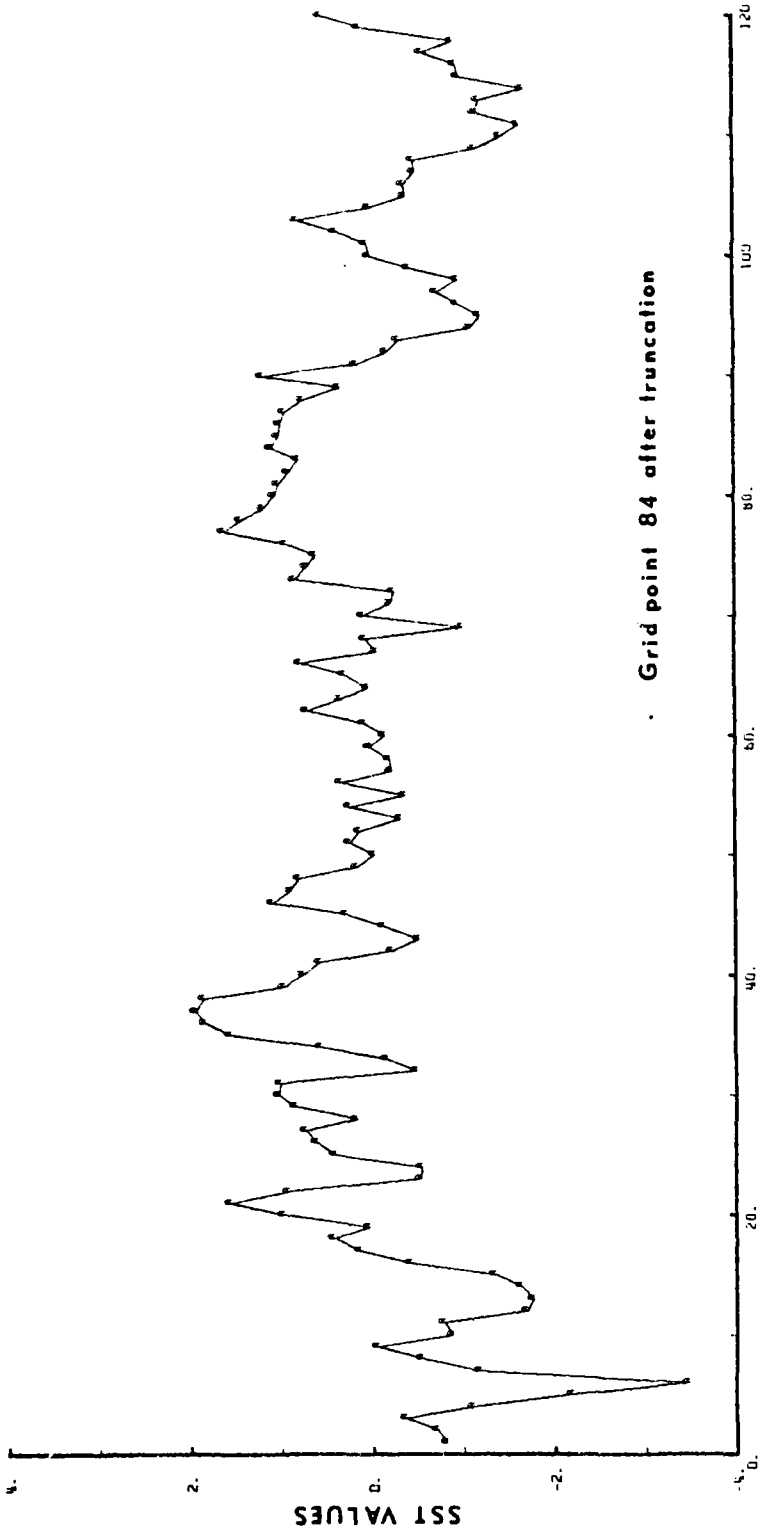


Figure 18. Same as Fig. 16 except for grid point 84.

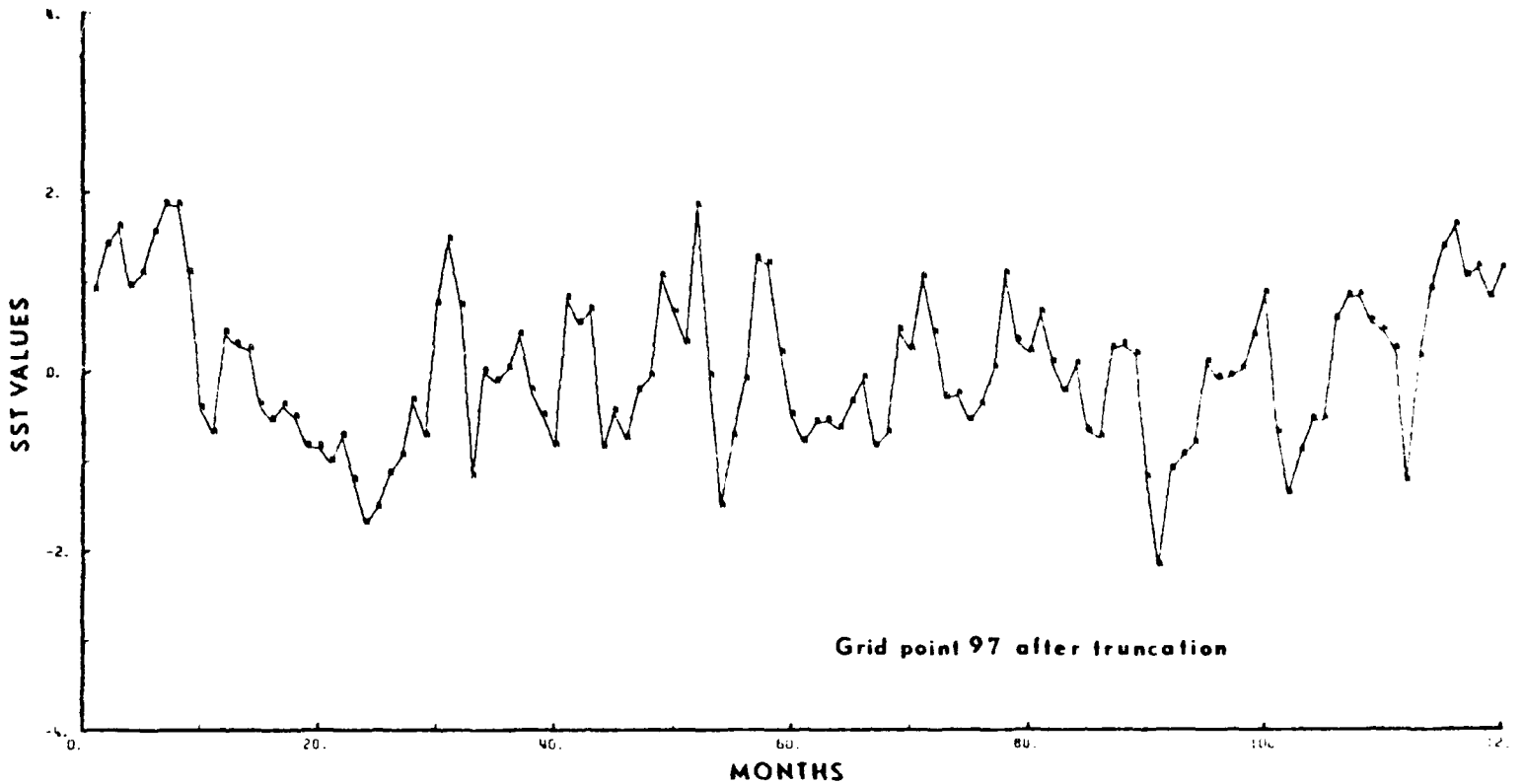


Figure 19. Same as Fig. 16 except for grid point 97.

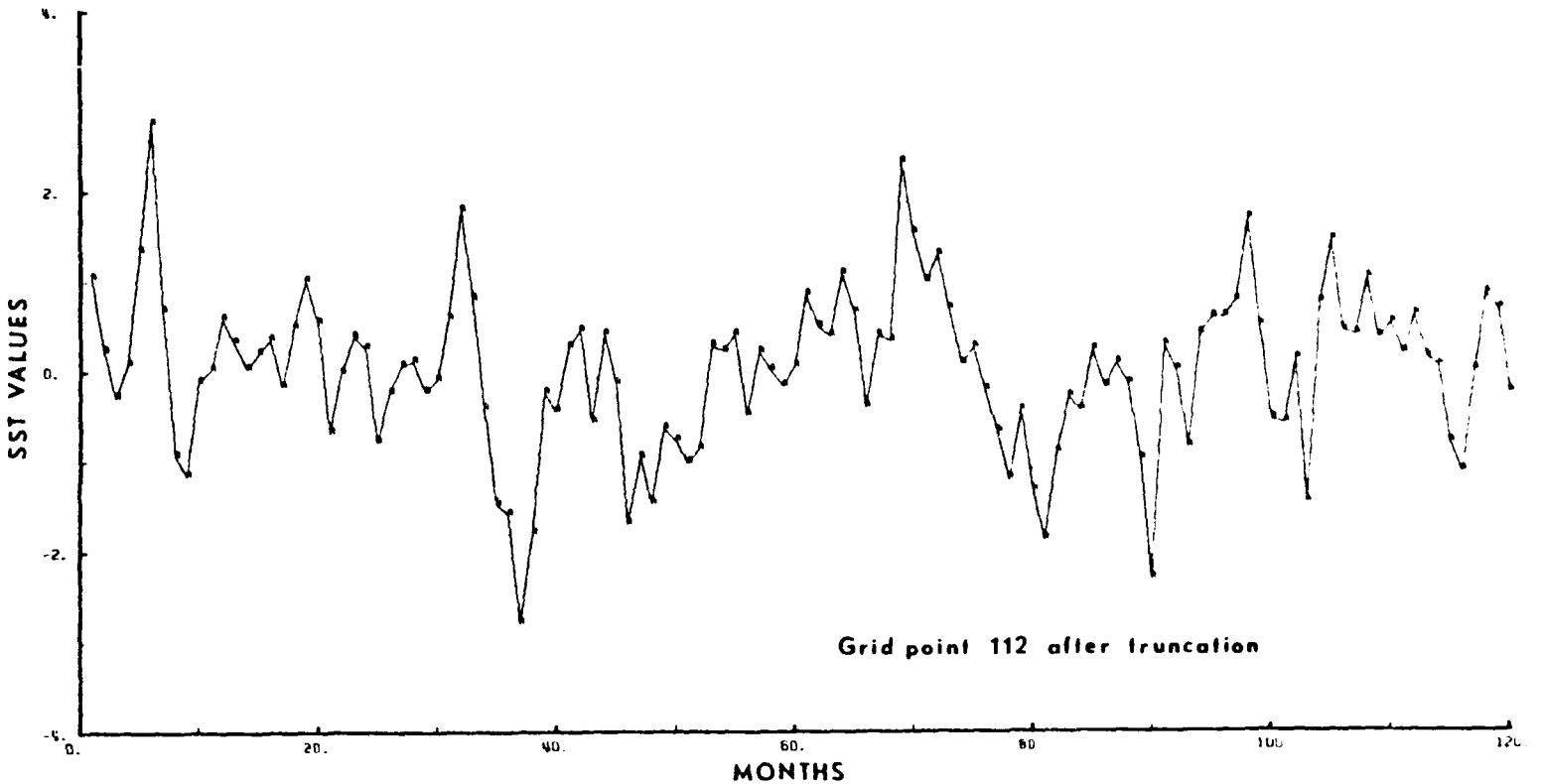


Figure 20. Same as Fig. 16 except for grid point 112.

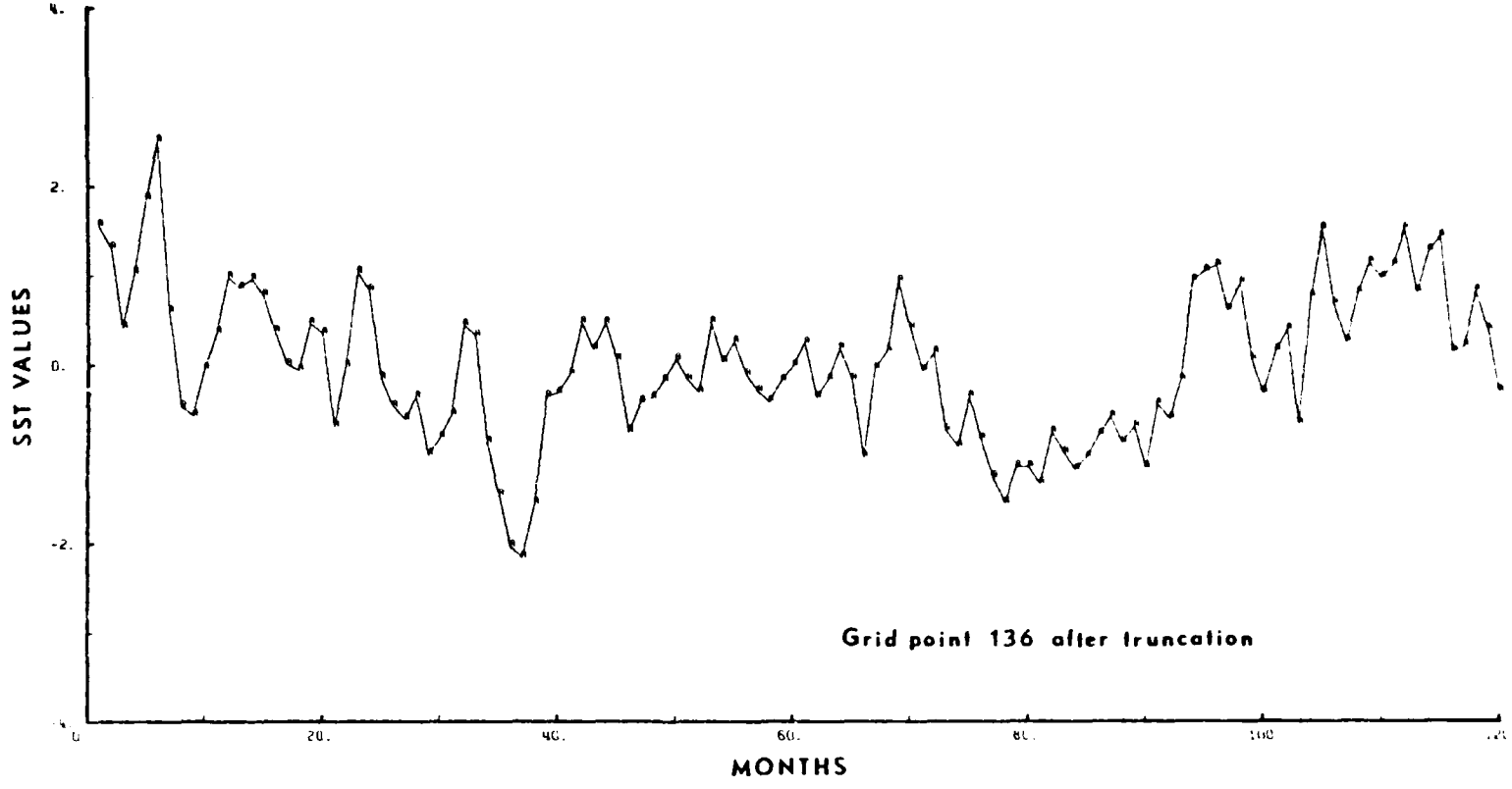


Figure 21. Same as Fig. 16 except for grid point 136.

TABLE III

Rcrit Computation Values from Several Random Grid Points

| Grid Point | n-Number of Events | Event Length (Months) | Rcrit |
|---|---|---|---|
| 21 | 27 | 4.4 | .19 |
| 55 | 29.5 | 4.0 | .18 |
| 84 | 26.5 | 4.5 | .19 |
| 97 | 28 | 4.3 | .19 |
| 112 | 34.5 | 3.5 | .17 |
| 136 | 30.5 | 3.9 | .18 |
| | | Average | .18 |

the values obtained from these calculations. The number of independent events, n, was estimated by averaging the number of peaks with the number of troughs in the time series. Dividing 120 months by n provided the average event length. The formula for Rcrit, the critical correlation value, was derived from Davis (1976) in the following form,

$$Rcrit = \frac{1}{\sqrt{n}} \qquad (4\text{-}1)$$

where n is again the number of independent events during the data record length. At any grid point, a correlation is considered significantly different from zero only if it exceeds Rcrit. The importance of these values of Rcrit will be discussed in a detailed examination of all the correlation maps in a following paragraph.

Sciremammano (1979) has described a method of presenting correlations which conveniently and accurately incorporate the significance of the correlation relative to the level of artificial correlation. The technique consists of normalizing (dividing) the raw correlations by their large-lag standard error ($\sigma_s$). This is defined from the Bartlett formula [Bartlett, 1978, p. 352] as

$$\sigma_s^2 = \left(\sum_{i=-\infty}^{\infty} C_{xx}(i\Delta t)\, C_{yy}(i\Delta t)\right)/N \qquad (4\text{-}2)$$

where $C_{xx}$ and $C_{yy}$ are the discrete autocorrelation functions of the variables x and y, respectively. It can be seen that (4-2) represents the ratio of a measure of the integral time scale of the variables x and y to the record length N. Thus, the normalization will compensate for the interplay of the dominant time scales of the input processes and the record length and will yield significance levels. Consideration of this interplay can be crucial when comparing meteorological and oceanic variables which, in general, have different time scales of variability. In the present study, such a presentation of the correlations would essentially give a more quantitative estimate of Rcrit than given above, and it would allow Rcrit to vary over the North Pacific, reflecting the fact that the dominant time scales of variability of SST and $u_*^3$ may, perhaps, not be uniform. These calculations were not made for this thesis and would offer an opportunity in a subsequent study to increase the value of the correlation maps. For the purpose of this thesis, a correlation, r, is considered significantly different from zero if $|r| > 0.20$.

In light of the previous comments, further review of the $u_*^3$ lag correlation maps and Table II will now reveal several additional interesting details. All maps reflect a large geographic scale of correlation compared to the total area of interest. The timing of the maximum magnitude of negative

area (NNEG) and maximum total negative correlation (RNEG) varies among the three data sets. Table II shows that $u_*^3$F1 has its maximum area of negative correlations at the zero month lag, while $u_*^3$F2 and $u_*^3$Fm have their max areas established at a plus-one-month lag. The maximum map sum of all negative correlations occurs at a plus-one-month lag for $u_*^3$F1 and $u_*^3$F2 and at a zero month lag for $u_*^3$Fm. The values of RNEG and NNEG attained by the $u_*^3$F2 data at a lag of plus one month exceeded all other data maps. Thus, it appears the $u_*^3$ verifies the expectation that anomalous storminess values, as reflected by $u_*^3$F2, are related to anomalous surface cooling with a time scale of two to six weeks.

It is interesting to note that if only correlations of absolute value greater than 0.20 are considered significant, then most of the trends indicated above remain in effect. For $u_*^3$F1 and $u_*^3$F2, the bulk of the positive correlation areas are not significant, while approximately half of the negative correlations (at lag of +1 month in Figure 15) are. The result appears to be, after considering all the possible significance checks provided previously and the map details delineated above, that at a plus-one-month lag there is a large mid-oceanic area where $u_*^3$F1 and $u_*^3$F2 acting as anomalous storminess variables produce a cooling of the sea surface. The mechanism responsible for this cooling most

likely is the vertical mixing (entrainment) of cold water from below the mixed-layer.

B. LARGE LAG CORRELATIONS BETWEEN $u_*^3$F1 AND SST

As an experiment to lend additional credibility to the large shift in correlations observed at the plus-one-month lag, an analysis was conducted by correlating the SST field with a wind parameter, specifically $u_*^3$F1, that occurred 12, 17, 21, 24, 29, and 36 months later. It was expected that the correlations obtained from this analysis would be non-significant and offer by their scale and magnitude some support for the previously described results. Figure 22 contains the correlation maps, from top to bottom, of minus 12, minus 24, and minus 36 months' lag and Figure 23 contains the correlation maps, from top to bottom, of minus 17, minus 21, and minus 29 months' lag. Examination of these two figures reveals that, in comparison to $u_*^3$F1 lagged plus one month, all maps have much smaller areas of negative correlations, although some areas are significant (greater than .20) by the earlier test.

Table IV which delineates the values of RNEG, NNEG, RPOS, and RSUM for $u_*^3$F1 at the trial lags examined indicates that the RNEG and NNEG values remain much below those values observed for $u_*^3$F1 at zero and plus-one-month lag.

The average RNEG is -7.67 and the average NNEG is 76 for lags of minus one to minus 36 months. Both values lie

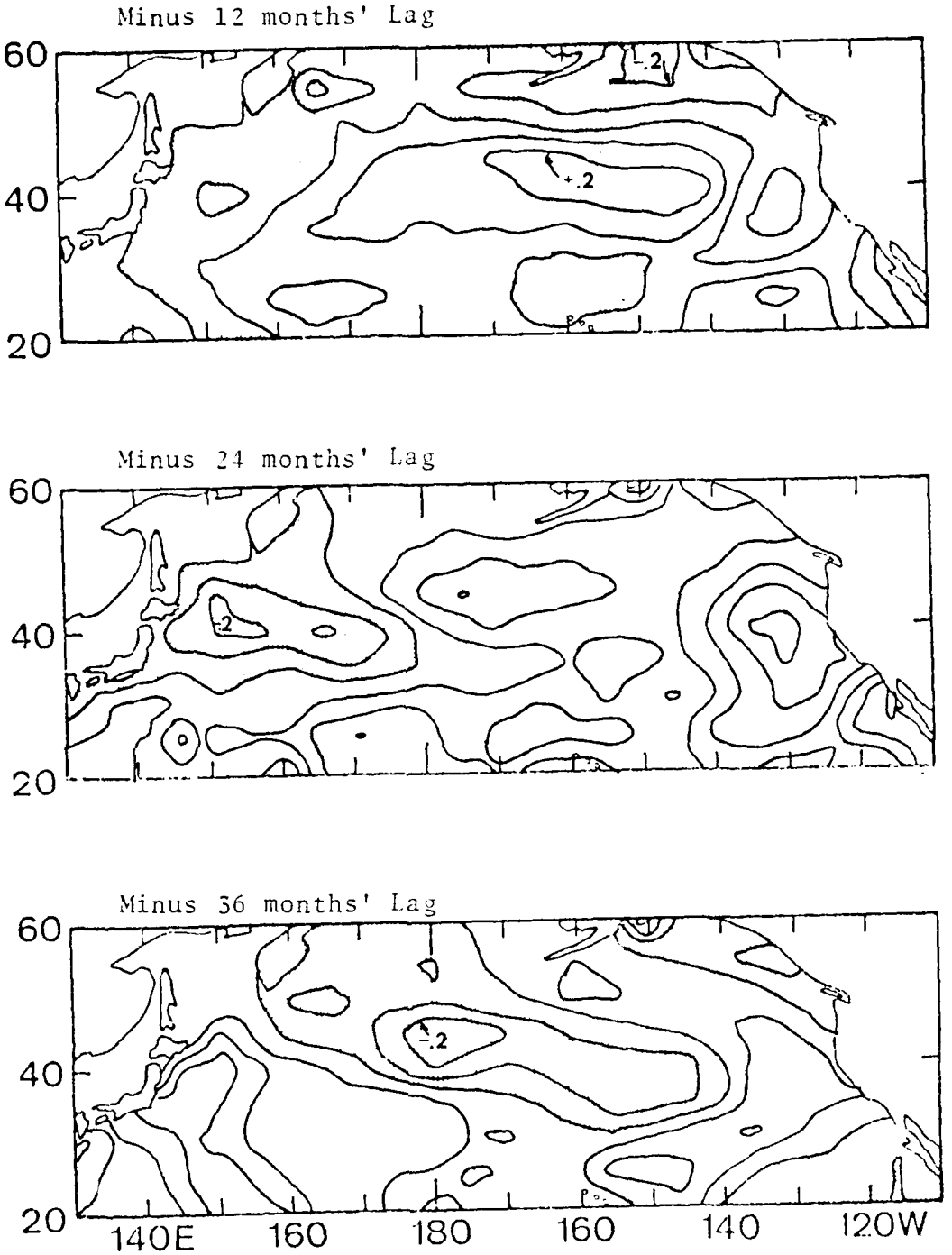


Figure 22. Correlation maps of $u_*^3$F1 and SST Anomaly fields for lags of minus 12, 24 and 36 months. The last closed isoline is labeled in some regions having the largest correlations.

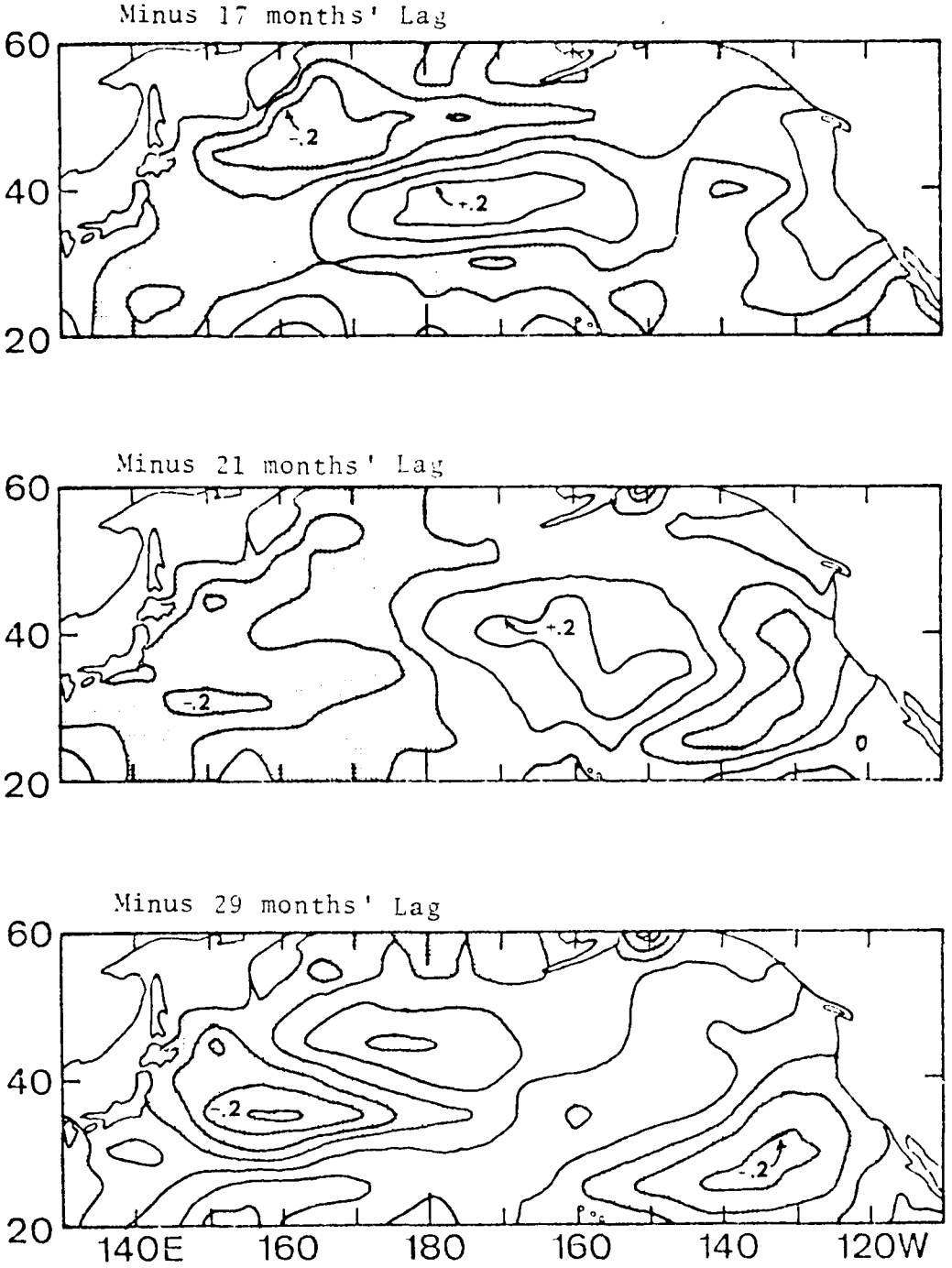


Figure 23. Same as Fig. 22 except for lags of minus 17, 21 and 29 months.

TABLE IV

CORRELATION MAP STATISTICS

FOR ANOMALOUS $u_*^3$F1 LAGGED WITH ANOMALOUS SST

| | LAG (Months) | | | | | | | | | |
|---|---|---|---|---|---|---|---|---|---|---|
| | -36 | -29 | -27 | -25 | -24 | -23 | -21 | -19 | -17 | -12 |
| RNEG | -5.84 | -7.16 | -8.15 | -3.69 | -4.96 | -5.43 | -8.71 | -11.35 | -8.00 | -5.23 |
| NNEG | 63 | 54 | 77 | 49 | 44 | 55 | 81 | 95 | 90 | 72 |
| RPOS | 17.21 | 13.28 | 8.51 | 15.08 | 18.32 | 16.29 | 10.06 | 6.32 | 8.45 | 10.61 |
| RSUM | 11.37 | 6.12 | 0.36 | 11.39 | 13.36 | 10.86 | 1.35 | -5.02 | 0.45 | 5.37 |

RNEG - Sum of Negative Correlations

NNEG - Number of Grid Points with a Negative Correlation

RPOS - Sum of Positive Correlations

RSUM - Arithmetic Sum of All Correlations

considerably below the values observed for $u_*^3$F1 at a plus-one-month lag, where RNEG was -24.96 and NNEG was 131.

C. LAG CORRELATIONS BETWEEN $curl_z\tau$ AND SST

Figures 24 to 30 are maps of lagged correlations between $curl_z\tau$ and SST over the same area as the previously viewed correlation maps of $u_*^3$ and SST. The layout of the maps is exactly the same as before with the maps progressing through lags of minus three to plus three months, in one-month increments with Figure 24 showing the minus-three-month case and Figure 30 ending the series with a plus-three-month lag between $curl_z\tau$ and SST. In this map series, as in the previous series, SST is lagged relative to $curl_z\tau$. Thus, the map with a lag of plus one month shows the correlation between the $curl_z\tau$ field and the SST field that occurred one month later. Each figure contains three maps, which are, from top to bottom, correlations between SST and (1) $curl_z\tau$F1 computed from high-pass wind components only, (2) $curl_z\tau$F2 computed from a combination of high- and low-pass components, and (3) $curl_z\tau$Fm computed from unfiltered (total) wind components, respectively. As before, each map is shaded gray in areas of negative correlation values.

Similar expectations existed for this set of correlation maps like those indicated before for $u_*^3$. That is, since anomalous values of wind stress curl indicate anomalous Ekman pumping, it was expected that for lags greater than or

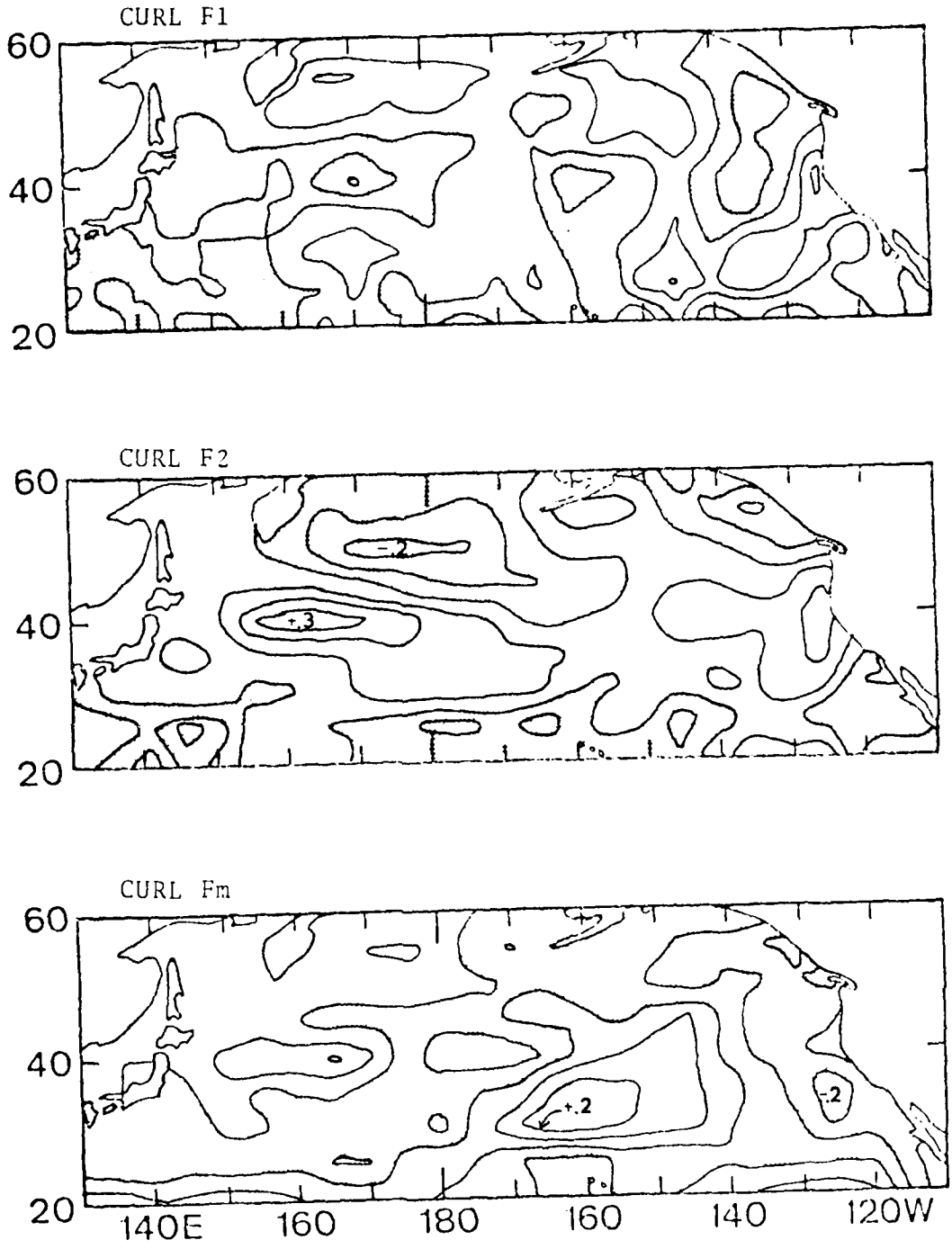


Figure 24. Correlation maps of the curl anomaly data fields with SST at a lag of minus three months. The last closed isoline is labeled in some regions having the largest correlations.

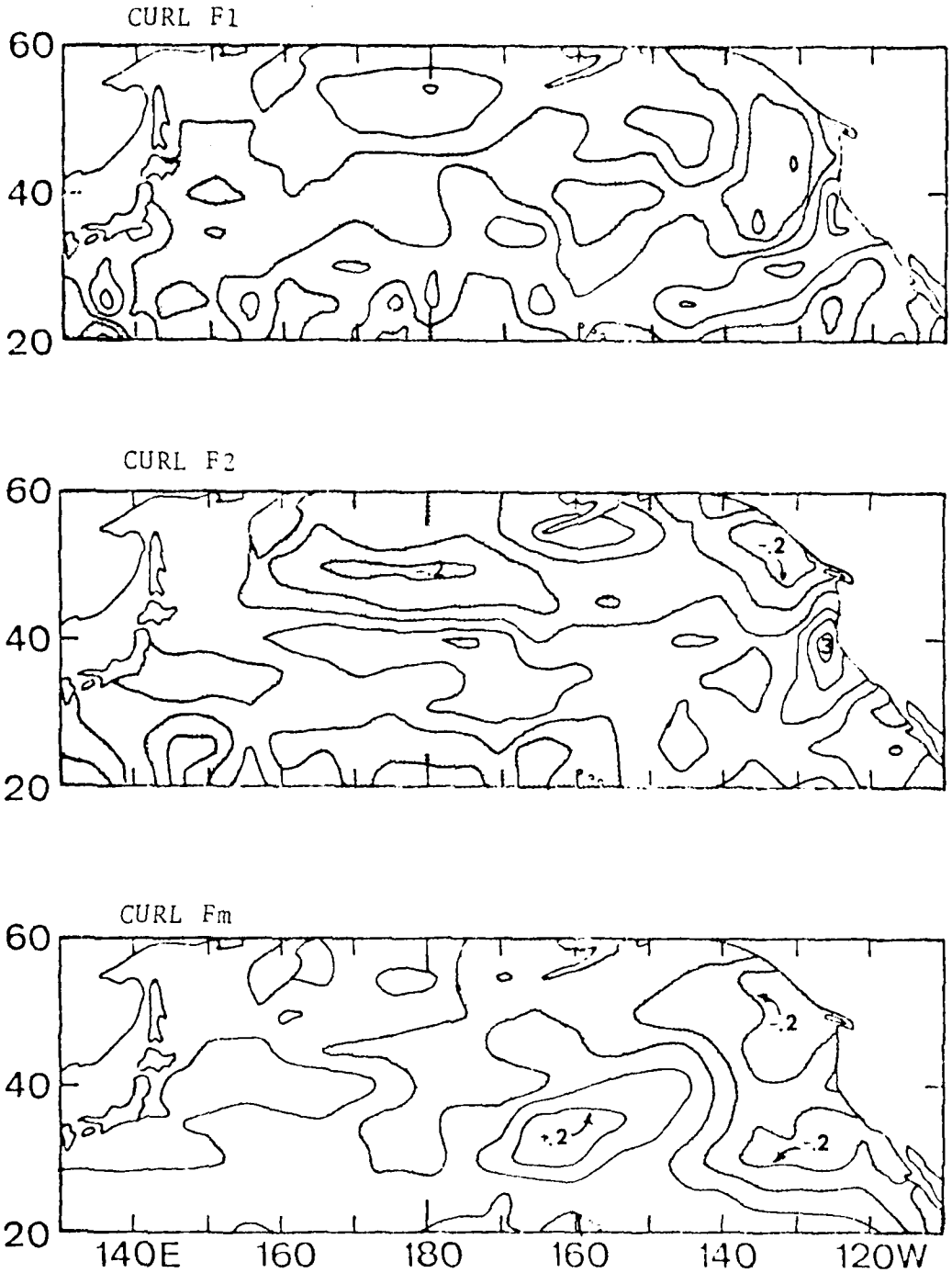


Figure 25. Same as Fig. 24 except lagged minus two months.

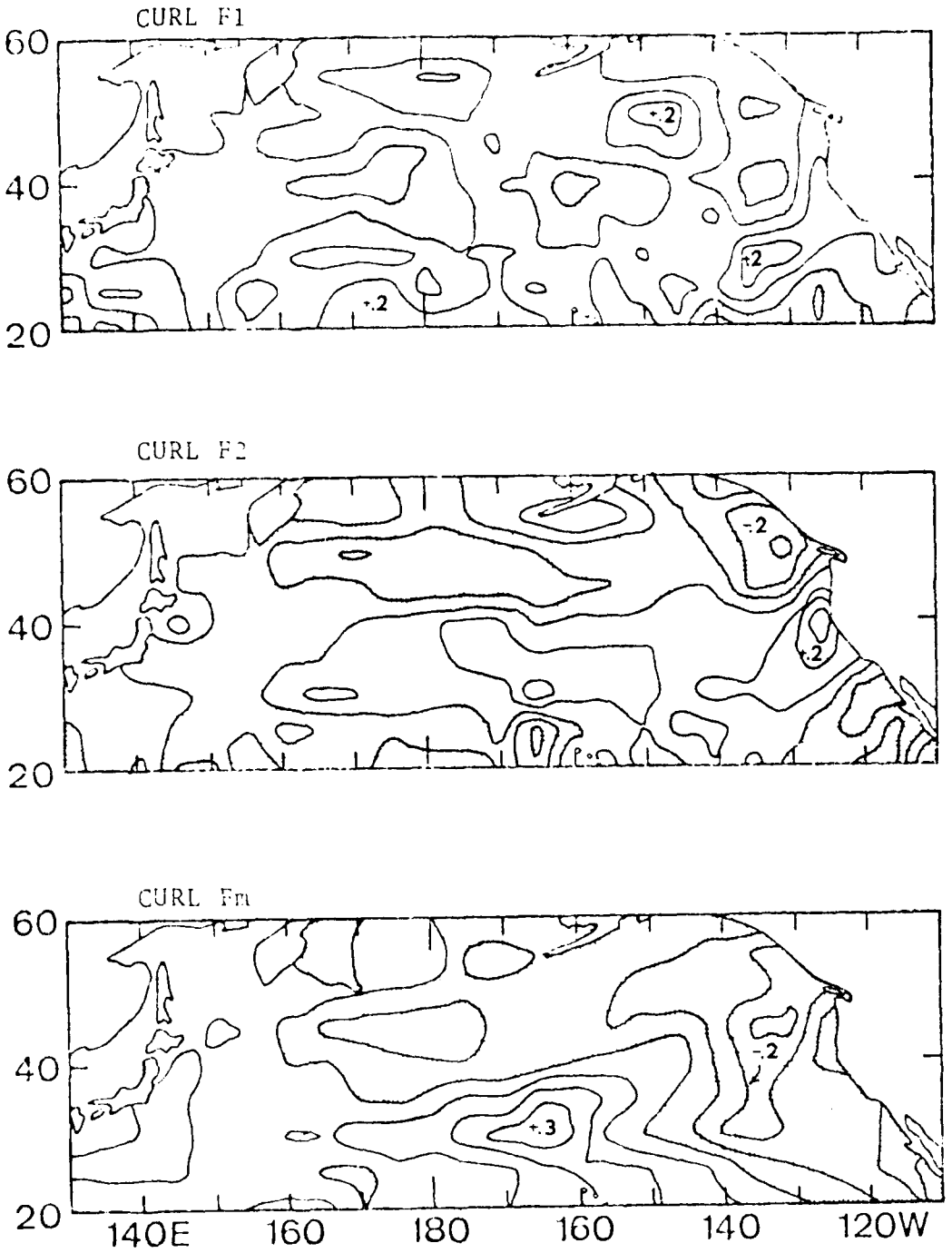


Figure 26. Same as Fig. 24 except lagged minus one month.

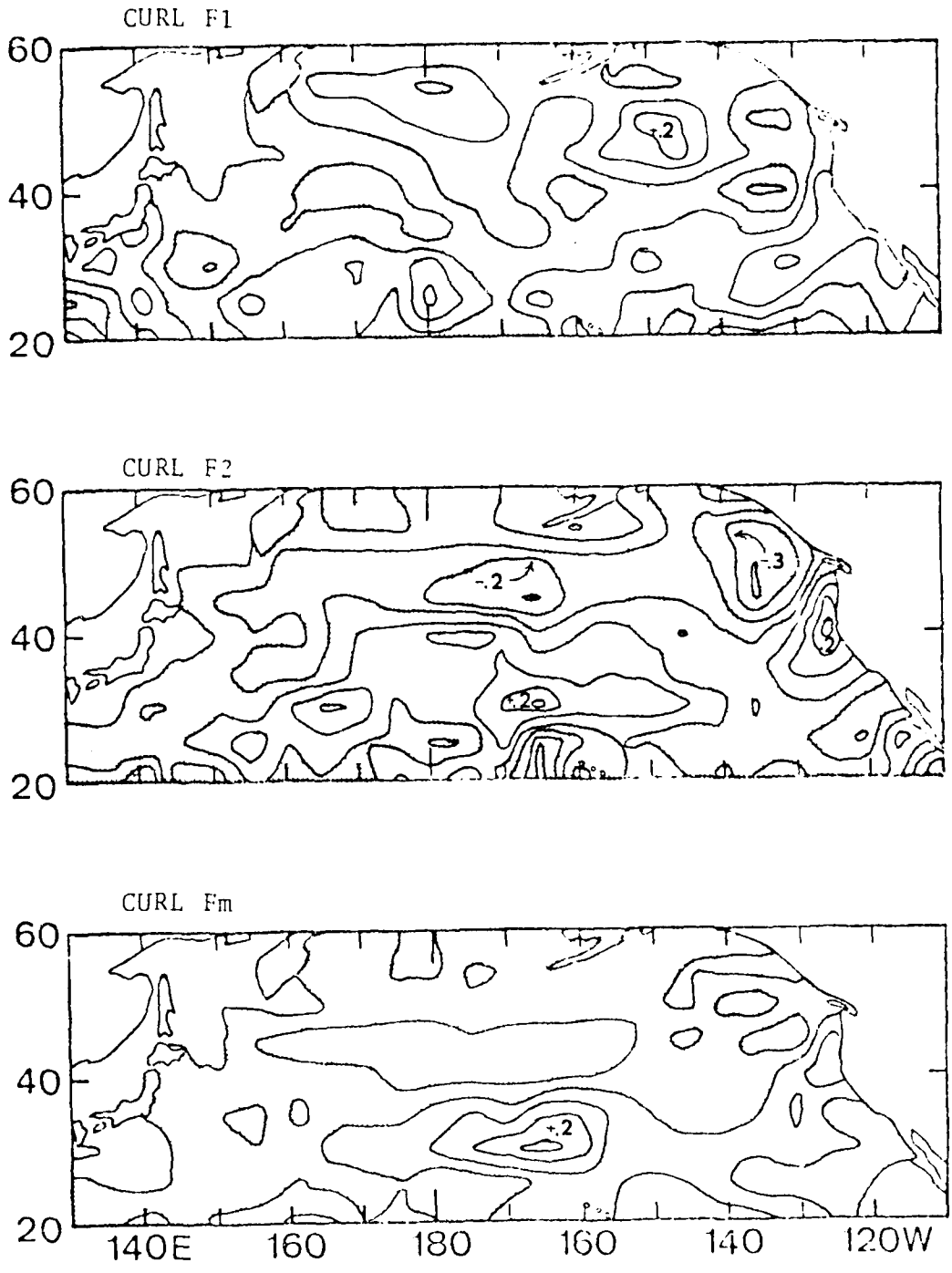


Figure 27. Same as Fig. 24 except no lag between data sets.

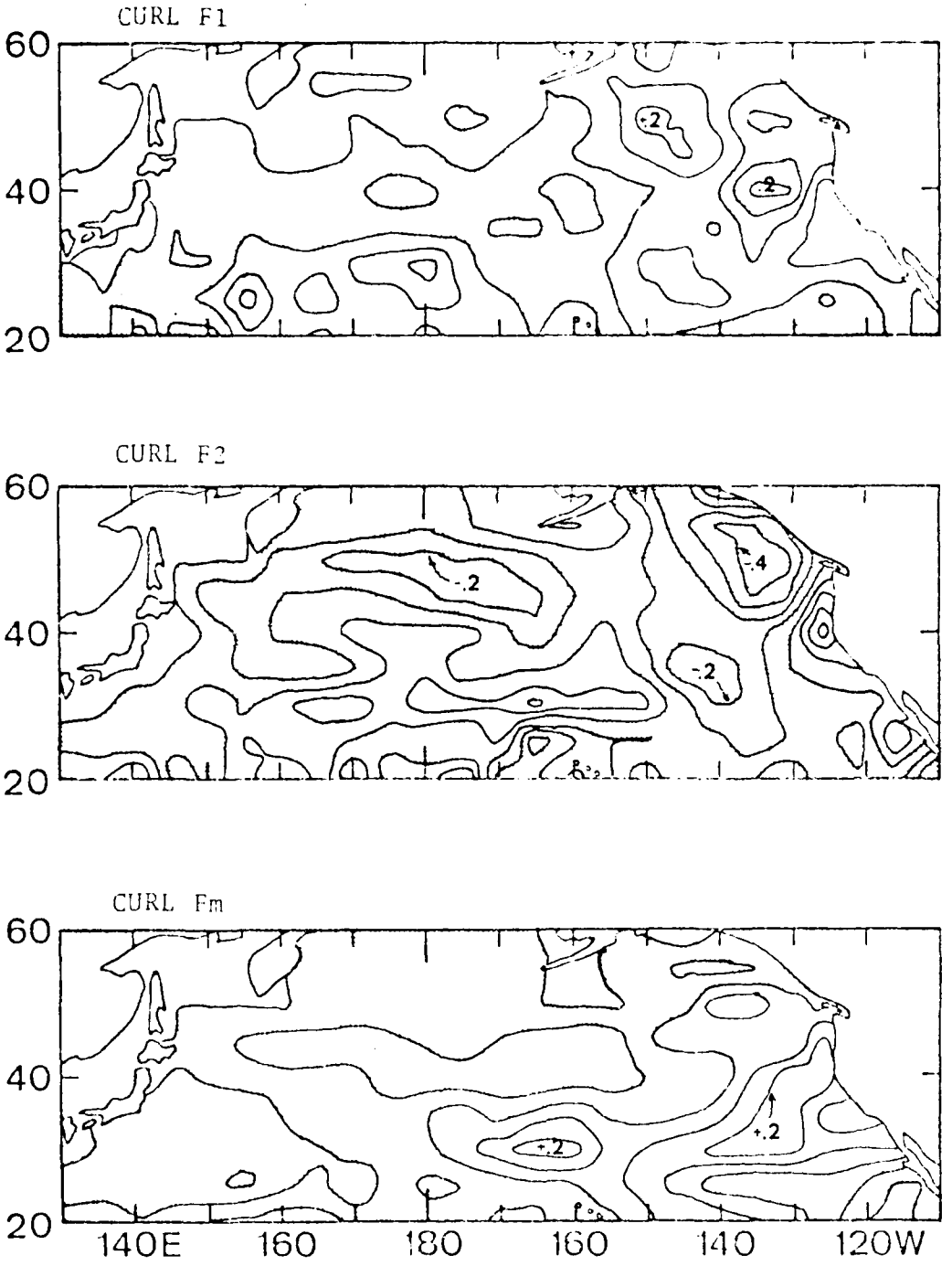


Figure 28. Same as Fig. 24 except lagged plus one month.

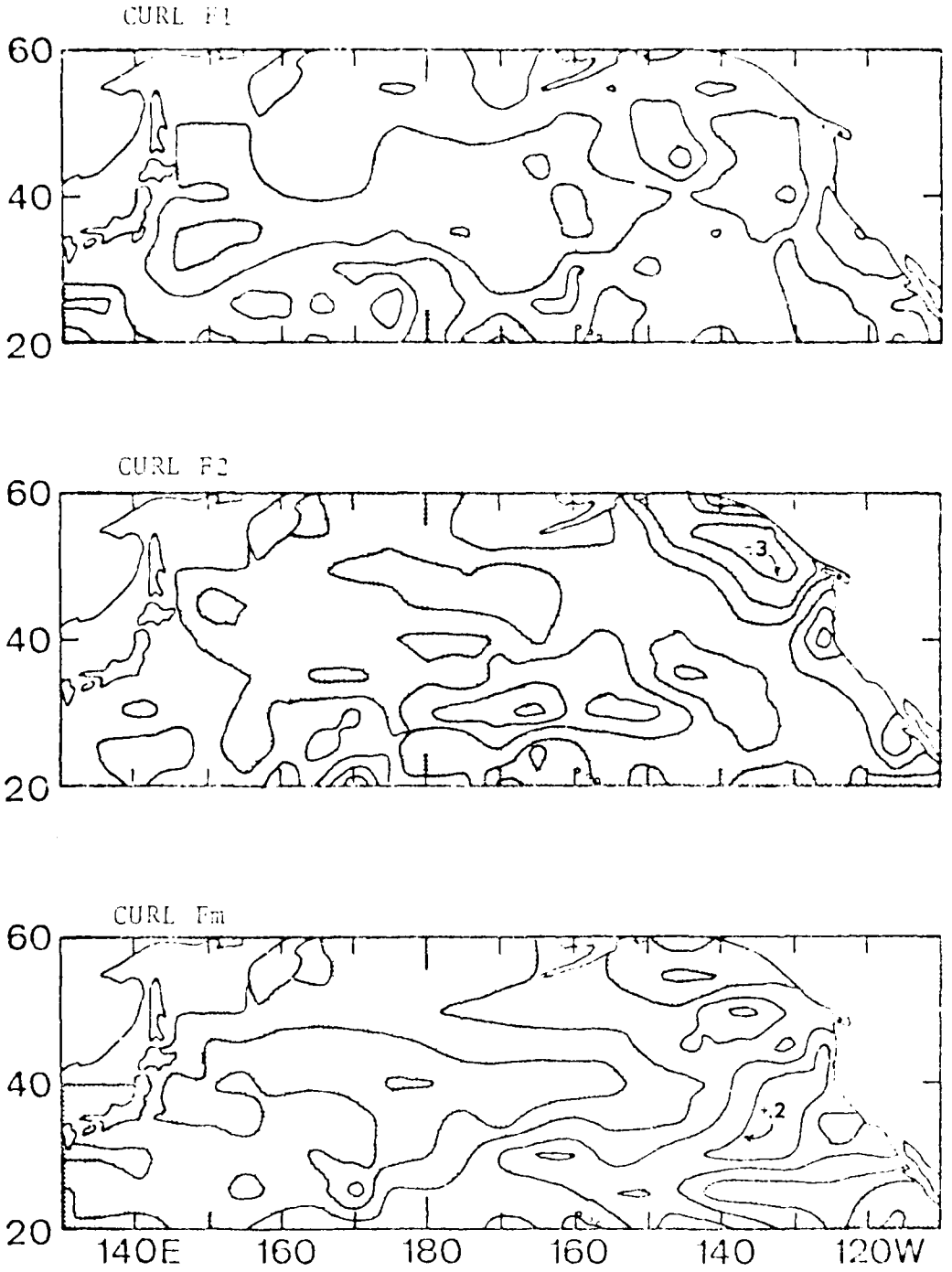


Figure 29. Same as Fig. 24 except lagged plus two months.

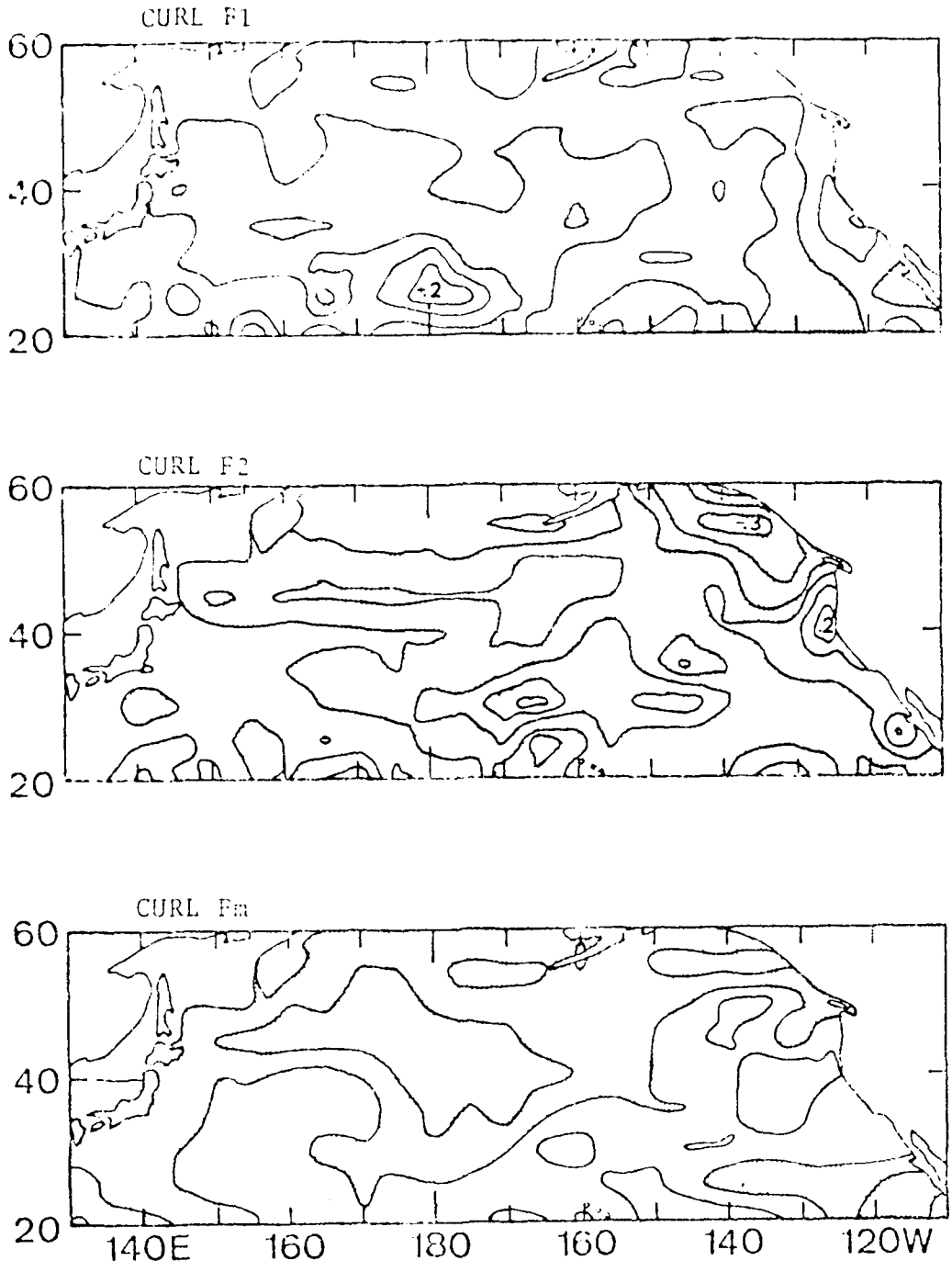


Figure 30. Same as Fig. 24 except lagged plus three months.

equal to zero, the maps would be mostly covered by negative correlation values. Examination of Figures 24 through 30 reveals that the correlations between $curl_z\tau$ and SST occur on a smaller geographic scale than the correlations between $u_*^3$ and SST. There is an increase in the amount of gray shaded area as the maps are viewed from minus three to plus three months lag with a maximum occurring at the zero or plus-one-month lag. This increasing gray shading trend is not as strong as that observed in the $u_*^3$ series and examination of Table V shows that the statistics used to quantify the correlations do not approach those values obtained from Table II, the $u_*^3$ measurements. Table V reveals that the max number of negative correlations (NNEG) is attained by the $curl_z\tau Fm$ field with a plus-one-month lag. The maximum magnitude of totaling all negative correlations (RNEG) is observed to occur at a plus-one-month lag in the $curl_z\tau F2$ field. Remembering that the random correlation situation would have a standard deviation of 6.5 grid points, both $curl_z\tau F2$ and $curl_z\tau Fm$ undergo shifts of approximately two standard deviations or more when the lag shifts from minus one to zero and from zero to plus one month lag. Thus there is a significant shift away from the possible random correlation case. When only the statistically significant correlations ($|r| > .20$) are considered, much smaller negative correlation areas result in Figure 28. These

TABLE V

CORRELATION MAP STATISTICS FOR ANOMALOUS CURL LAGGED WITH ANOMALOUS SST

| | | LAG (MONTHS) | | | | | | |
|---|---|---|---|---|---|---|---|---|
| | | -3 | -2 | -1 | 0 | +1 | +2 | +3 |
| RNEG | $curl_z \tau F1$ | -6.42 | -6.83 | -5.57 | -6.74 | -5.60 | -4.54 | -5.13 |
| | $curl_z \tau F2$ | -7.60 | -8.34 | -8.59 | -13.20 | -15.79 | -10.84 | -9.17 |
| | $curl_z \tau Fm$ | -9.70 | -8.50 | -10.72 | -8.19 | -11.70 | -9.26 | -7.19 |
| NNEG | $curl_z \tau F1$ | 77 | 80 | 78 | 81 | 77 | 66 | 77 |
| | $curl_z \tau F2$ | 72 | 82 | 85 | 100 | 112 | 99 | 92 |
| | $curl_z \tau Fm$ | 99 | 74 | 88 | 103 | 114 | 97 | 92 |
| RPOS | $curl_z \tau F1$ | 8.10 | 8.03 | 8.18 | 8.05 | 7.97 | 7.57 | 6.75 |
| | $curl_z \tau F2$ | 10.22 | 8.11 | 8.14 | 6.64 | 5.67 | 5.60 | 6.23 |
| | $curl_z \tau Fm$ | 7.28 | 8.75 | 10.71 | 5.72 | 6.53 | 7.92 | 5.95 |
| RSUM | $curl_z \tau F1$ | 1.68 | 1.20 | 2.61 | 1.31 | 2.37 | 3.03 | 1.63 |
| | $curl_z \tau F2$ | 2.62 | -.23 | -.45 | -6.56 | -10.12 | -5.24 | -2.94 |
| | $curl_z \tau Fm$ | -2.42 | .25 | -.01 | -2.47 | -5.17 | -1.33 | -1.95 |

RNEG - Sum of Negative Correlations
NNEG - Number of Grid Points with a Negative Correlation
RPOS - Sum of Positive Correlations
RSUM - Arithmetic Sum of All Correlations

"significant" areas are small and scattered. In the $curl_z \tau^{P2}$ field, a negative correlation area persists off the West Coast of Canada with a maximum size and strength at plus one lag. In general, the significance of the relationship between SST and $curl_z \tau$ appears to be somewhat less than that between SST and $u_*^3$.

# V. CONCLUSIONS

The primary hypothesis that was tested in this study was that the sea surface temperature (SST) responds to atmospheric wind forcing, as manifested in storms, and that the amount of response is proportional to the amount of wind forcing. When the atmospheric forcing is characterized as an anomalous storminess and calculated as $u_*^3$ and $\mathrm{curl}_z \tau$, it has a negative correlation with anomalous SST over most of the North Pacific at a plus-one-month lag. It appears that $u_*^3$ is more strongly related to SST anomalies than is $\mathrm{curl}_z \tau$. Thus, vertical mixing may be a stronger influence than Ekman divergence and convergence in surface cooling. However, this difference could be caused by difficulties inherent in computing curl [Saunders, 1976].

Another conclusion concerns the compensation required to validate the magnitudes of the map correlations. The relatively short length of record (120 months) necessitates a calculation of the artificial correlation and a significant reduction in the computed correlations. Any increase in the record length will reduce the level of artificial correlation for this type of study [see (4-1)], but to make a significant increase in the total validity, a doubling or quadrupling of the total record length is necessary.

The present study examined the relationships between the atmosphere and ocean that exists throughout the year. It is now well known [Davis, 1978] that many ocean-atmospheric relationships are strongly seasonally dependent. It is possible that if the data of this study were stratified into seasons, statistically significant results could be obtained. The problem of artificial correlation would increase because of fewer independent events [n in Table III and (4-1)] available for correlation, but the actual correlations could possibly increase enormously. For example, the relation of the winter anomalous storminess with anomalous sea surface temperature cooling has the potential to be much more significantly correlated than the non-seasonal relations developed in this research.

Whenever one endeavors in a study of this sort, more questions are often generated than answers found. One remaining question is, What can the wind alone tell about the future state of the ocean? That is, perhaps $u_*^3$ and $\text{curl}_z \tau$ are sufficiently uncorrelated that they <u>together</u> may be more significantly correlated with SST. It is recommended therefore that a further study correlating SST with a combined form of $u_*^3$ and $\text{curl}_z \tau$ be done in order to provide a more complete answer to this question. This will give a more complete estimate of the total importance of the winds, relative to other effects, in changing the SST.

# APPENDIX

Methods for representing arrays of environmental variables by empirical orthogonal functions have been formulated in a number of different ways. [See, for example, Lorenz, 1956; Kutzbach, 1967; Stidd, 1967; Davis, 1976.] Most of the information presented in this appendix is based upon the work of Kutzbach (1967).

Let $A_n$ be a P component vector which represents the $n^{th}$ (n = 1...., N) observation of P variables and let A be a P by N matrix, where the $n^{th}$ column is the observation vector $A_n$. The goal is to determine a vector e which has the highest degree of similarity to all the $A_n$ observation vectors simultaneously. Kutzbach (1967) explains that if the similarity is measured with the squared and normalized inner product between the observation vectors $A_n$ and the determined vector e, the problem is to maximize

$$(e'A)^2 N^{-1}/e'e = \frac{(e'A)(e'A)'}{Ne'e} = \frac{e'AA'e}{Ne'e}$$

after averaging across all $A_n$. The prime denotes the transpose. This is equivalent to maximizing

$$e' Be \ , \qquad (1\text{-}1)$$

subject to the condition

$$e' e = 1 , \qquad (1\text{-}2)$$

where B is an m by m symmetric matrix whose $b_{ij}^{th}$ element is given by

$$b_{ij} = N^{-1} \sum_{n=1}^{N} A_{in} A_{jn} ,$$

$$B = N^{-1} (A'A) , \qquad (1\text{-}3)$$

and m is the larger of P and N.

Furthermore, Kutzbach (1967) continues by pointing out that the maximization of (1-1) subject to (1-2) leads to the equation

$$Be = e\lambda . \qquad (1\text{-}4)$$

The vector e and the parameter $\lambda$ can now be recognized as an eigenvector and associated eigenvalue of the symmetric normalized matrix B. It can be shown that the $e_i$ are orthogonal and the $\lambda_i$ are real and positive. Therefore, (1-4) can be rewritten as

$$BE = EL \qquad (1\text{-}5)$$

where E is the m by m matrix of eigenvectors and L is the m by m diagonal matrix of eigenvalues. Note that

$$E'E = I \ . \tag{1-6}$$

In the following, it is assumed that the elements of L and the columns of E have been arranged such that $e_1$ is associated with $\lambda_1$, the largest eigenvalue of B, $e_2$, is associated with $\lambda_2$, the next largest eigenvalue of B, and so forth. Combining (1-5) and (1-5), and noting from (1-6) that for orthogonal matrices the transpose is equal to the inverse, one obtains

$$E'AA'E = LN \tag{1-7}$$

defining

$$E = E'A \tag{1-8}$$

where C is an m by m matrix, it follows that

$$A = EC \tag{1-9}$$

and

$$A_n = \sum_{i=1}^{m} c_{in} e_i, \quad n=1...., N. \tag{1-10}$$

Examination of (1-10) reveals that the observation vector $A_n$ can be expressed as a linear combination of the m eigenvectors. If all m eigenvectors are used, then the observation vector $A_n$ is exactly reproduced.

In most applications of empirical orthogonal function to non-random data, it is found that a large portion of the variance can be accounted for by retaining only the first few largest eigenvalues and related eigenvectors. Thus, retaining only the first few terms of (1-10) approximates the observation vector. If $A_n^*$ is defined as the approximation to the $n^{th}$ observation vector, then

$$A_n^* = \sum_{i=1}^{P^*} c_{in} e_i, \quad n=1,\ldots,N; \quad P^* < P . \qquad (1\text{-}11)$$

This allows truncation of noise by removing those terms with small variances. These smaller terms are most likely to consist almost entirely of noise as shown by the work of Preisendorfer and Barnett (1977).

Specific application of the preceding is delineated below, using SST data, in an outline detailing the array sizes and IBM-360 IMSL routines. Note: Only the truncation limits (the value of $P^*$) varied among the data sets and P = 166 grid points with N = 120 observations.

| ARRAY | NAME | COMPUTER ROUTINE |
|---|---|---|
| A (120 x 166) | Anomalous Data Set | |
| A'A (166 x 120)(120 x 166) | Transpose Product | VTPROF |
| B (166 x 166)/120 | Normalized Symmetric Matrix | |
| L (166 x 166) | Eigenvalues | EIGRS |
| E (166 x 166) | Eigenfactors | EIGRS |
| E (166 x 12) | Truncated Eigenvectors | |
| C (120 x 12) | Time Coefficients | VMULFF |
| $A^*$ (120 x 166) | Approximated Data Set | VMULFP |

LIST OF REFERENCES


Bartlett, M. S., 1978: An Introduction to Stochastic Processes. Cambridge University Press, 362 pp.

Beale, E. M. L., M. Kendall, and D. Mann, 1967: The Discarding of Variables in Multivariate Analysis. Biometrika, 54, 357.

Brier, G. W. and G. Meltesen, 1976: Eigenvector Analysis for Prediction of Time Series. J. Appl. Meteor., 15, 1307-1312.

Buell, C. E., 1978: The Number of Significant Proper Functions of Two-Dimensional Fields. J. Appl. Meteor., 17, 717-722.

Craddock, J. M., and C. Flood, 1969: Eigenvectors for Representing the 500mb Geopotential Surface over the Northern Hemisphere. Quart. J. Roy. Meteor. Soc., 95, 576-593.

Davis, R. E., 1976: Predictability of Sea Surface Temperature and Sea Level Pressure Anomalies over the North Pacific Ocean. J. Phys. Oceanogr., 6, 249-266.

Davis, R. E., 1978: Predictability of Sea Level Pressure Anomalies over the North Pacific Ocean. J. Phys. Oceanogr., 8, 233-246.

Dyer, T. D., 1975: The Assignment of Rainfall Stations into Homogeneous Groups: An Application of Principal Components. Quart. J. Roy. Meteor. Soc., 101, 1005-1013.

Elsberry, R. L. and N. Camp, 1978: Oceanic Thermal Response to Strong Atmospheric Forcing I. Characteristics of Forcing Events, J. Phys. Oceanogr., 8, 206-214.

Essenwanger, D., 1976: Applied Statistics in Atmospheric Science, Elsevier Scientific, Amsterdam, 412 pp.

Farmer, S., 1971: An Investigation into the Results of Principal Component Analysis of Data Derived from Random Numbers. The Statistician, 20, 63-72.

Fissel, D. B., S. Pond and M. Miyake, 1977: Computation of Surface Fluxes from Climatological and Synoptic Data, Mon. Wea. Rev., 105, 26-36.

Haney, R. L., M. S. Risch and G. Heise, 1980: A Climatological Study of the Wind Forcing due to Synoptic Storm Activity over the North Pacific Ocean (in preparation).

Harr, P. A., 1979: Relationships between Precipitation, Pressure and Ocean Temperature. Environmental Research Papers, Colorado State University, 19, 42 pp.

Kutzbach, J. E., 1967: Empirical Eigenvectors of Sea-Level Pressure, Surface Temperature and Precipitation Complexes over North America. J. Appl. Meteor., 6, 791-802.

Lorenz, E. N., 1956: Empirical Orthogonal Functions and Statistical Weather Prediction. M.I.T. Dept. of Meteor., Sci. Rept. No. 1, Contract AF19(604)-1566, 49 pp (Available from the Clearinghouse for Federal Scientific and Technical Information, U.S. Dept. of Commerce, Washington, D.C., Ad 110268.)

Preisendorfer, R. W., and T. Barnett, 1977: Significance Tests for Empirical Orthogonal Functions. 5th Conf. on Prob. and Statis. in Atmos. Sci., Nov 15-18, 1977, Amer. Meteor. Soc., Boston, MS, 169-172.

Rinne, J., and S. Järvenoja, 1979: Truncation of the EOF Series Representing 500mb Heights. Quart. J. Roy. Meteor. Soc., 105, 885-897.

Rinne, J., and V. Karhila, 1979: Empirical Orthogonal Functions of 500mb Height in the Northern Hemisphere Determined from a Large Data Sample. Quart. J. Roy. Meteor. Soc., 105, 873-884.

Risch, M. S., 1980: A Climatological Study of the Forcing of the North Pacific Ocean by Synoptic Storm Activity. M.S. Thesis, Naval Postgraduate School, Monterey.

Saunders, P. M., 1976: On the Uncertainty of Wind Stress Curl Calculations. J. Mar. Res., 34, 155-160.

Sciremammano, F., Jr., 1979: A Suggestion for the Presentation of Correlations and their Significance Levels. J. Phys. Oceanogr., 9, 1273-1276.

Simpson, J., 1969: On Some Aspects of Sea-Air Interaction in Middle Latitudes. Deep Sea Res., 16, 255-261.

Stidd, C. K., 1967: The Use of Eigenvectors for Climatic Estimates. J. Appl. Meteor., 6, 255-264.

Weare, B. C., 1979: A Statistical Study of the Relationships between Ocean Surface Temperatures and the Indian Monsoon. J. Atmos. Sci., 36, 2279-2291.

Weare, B. C., A. Navato and R. Newell, 1975: Empirical Orthogonal Analysis of Pacific Sea Surface Temperatures. J. Phys. Oceanogr., 6, 671-678.

# INITIAL DISTRIBUTION LIST

| | | No. Copies |
|---|---|---|
| 1. | Defense Technical Information Center<br>Cameron Station<br>Alexandria, Virginia 22314 | 2 |
| 2. | Library, Code 0142<br>Naval Postgraduate School<br>Monterey, California 93940 | 2 |
| 3. | Department Chairman, Code 63<br>Department of Meteorology<br>Naval Postgraduate School<br>Monterey, California 93940 | 1 |
| 4. | Assoc Professor R. L. Haney, Code 63 Hy<br>Department of Meteorology<br>Naval Postgraduate School<br>Monterey, California 93940 | 2 |
| 5. | Professor C. N. K. Mooers, Code 68 Mr<br>Department of Oceanography<br>Naval Postgraduate School<br>Monterey, California 93940 | 1 |
| 6. | Professor W. Van der Bijl, Code 63 Vb<br>Department of Meteorology<br>Naval Postgraduate School<br>Monterey, California 93940 | 1 |
| 7. | Department of Meteorology Library, Code 63<br>Naval Postgraduate School<br>Monterey, California 93940 | 1 |
| 8. | Professor R. H. Bourke, Code 68 Bf<br>Department of Oceanography<br>Naval Postgraduate School<br>Monterey, California 93940 | 1 |
| 9. | Commander<br>Naval Oceanography Command<br>NSTL Station, Mississippi 39529 | 1 |

| | | |
|---|---|---|
| 10. | Commanding Officer<br>Fleet Numerical Oceanography Center<br>Monterey, California 93940 | 1 |
| 11. | Officer-in-Charge<br>Naval Environmental Prediction<br>Research Facility<br>Monterey, California 93940 | 1 |
| 12. | Dr. Jerome Namias<br>NORPAX A-024<br>Scripps Institution of Oceanography<br>La Jolla, California 92093 | 1 |
| 13. | Dr. Tim Barnett<br>NORPAX A-024<br>Scripps Institution of Oceanography<br>La Jolla, California 92093 | 1 |
| 14. | Dr. Don Gillman<br>National Meteorological Center<br>National Weather Service, NOAA<br>Washington, D.C. 20233 | 1 |
| 15. | Dr. R. Preisendorfer<br>NOAA/PMEL<br>3711 15th Avenue, NE<br>Seattle, Washington 98105 | 1 |
| 16. | Mr. Patrick Harr<br>Control Data Corporation<br>205 Montecito Avenue<br>Monterey, California 93940 | 1 |
| 17. | LCDR William H. Little<br>5135 SW Sherwood Place<br>Beaverton, Oregon 97005 | 2 |

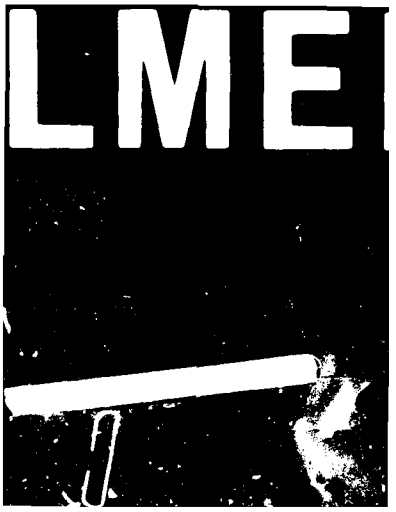
LME